THE SOURCE OF TOXICITY IN CTAB AND CTAB-STABILIZED GOLD NANORODS

By

David Schachter

A thesis submitted to the

Graduate School-New Brunswick

Rutgers, The State University of New Jersey

and

The Graduate School of Biomedical Sciences

University of Medicine and Dentistry of New Jersey

In partial fulfillment of the requirements

For the degree of

Master of Science

Graduate Program in Biomedical Engineering

Written under the direction of

Dr. Laura Fabris

And approved by

_____

_____

_____

New Brunswick, New Jersey

January 2013

ABSTRACT OF THE THESIS

THE SOURCE OF TOXICITY IN CTAB AND CTAB-STABILIZED GOLD NANORODS

By David Schachter

Thesis Director:
Laura Fabris, Ph.D.

The use of nanoparticles for sensing, cell imaging, and therapy has seen an extraordinary increase, in recent years. But, one of the issues commonly encountered when using nanoparticles in bioapplications is their toxicity.

Cetyltrimethylammonium bromide (CTAB) is a common surfactant used in nanoparticle synthesis. One of CTAB's uses is to direct the growth and stabilize the shape of certain types of colloidal metallic nanoparticles, for example gold nanorods. The main drawback is that these metallic nanoparticles cannot be used in applications with cells because of their cytotoxicity. Despite many conjectures, it is not yet clear what the origin of this cytotoxicity is. Here we explore some possible reasons and mechanisms that could be accounted for to explain this cytotoxicity.

Due to its molecular structure, CTAB is difficult to detect in solution using conventional methods. In this thesis work, electrospray ionization mass spectrometry (ESI-MS) was used as a means to detect CTAB in solution and *in vitro* and to study the source of its toxicity. From the data collected, we have evidence that there are two active mechanisms: 1) CTAB's interaction with the

phospholipid bilayer that destabilizes the cell membrane leading to cell death, and 2) the catalytic action of one of CTAB's dissociation products, the CTA+ cation, which might cause the quenching of the enzyme ATPsynthase and thus lead to energy deprivation and death of the cell. Our results also indicate that it is this second mechanism, which depends on the concentration of CTA+, to be the most lethal.

We have found that nanorods can be successfully formed with high concentrations of Br-, which is non-toxic, with limited amounts of CTAB, because CTA+ might be playing a more important role only for stability purposes. This will reduce the amount of CTAB in solution to below cytotoxic values. We have also found out that once the nanorods are formed using CTAB as the stabilizing surfactant, low concentrations of an iodine/iodide mixture are able to modify, post-fabrication, the aspect ratio of the nanorods and thus their optical properties. This discovery might lead to the development of a new category of gold nanorods, with decreased toxicity and tunable morphology that would be ideal for applications in conjunction to cells.

Acknowledgments:

I would like to thank Dr. Laura Fabris and the Fabris group including Swarnapali “Pali” Indrasekara, Paul Mark, Robert Wadams, Riyanka Pai, and Sara Nizzero for their assistance and discussion in developing this thesis. Also, I would like to thank Prof. Prabhas Moghe and Prof. Charles Roth for allowing me to access their labs and for providing the cell lines (U87 and A172) used in this research, and Dr. Dominik Naczynski and Ms. Margot Zevon for their assistance with the cell culture part of this work.

I would also like to express my thanks to Prof. Kathryn Uhrich, Prof. Stavroula Sofou, and Prof. Larry Romsted, for being part of my thesis committee and for all their support in this process.

Lastly, I would like to acknowledge my family for all the support they have given me. Specifically, my wife and son: My wife for always being there when I got frustrated, and my son for always smiling.

Dedication:

I would like to dedicate this thesis to my son, Aharon, and his future siblings. I finished writing this thesis and defended the thesis during the Jewish holiday of Hanukkah, which is the holiday in which the Jews celebrate defeating the Hellenist Greeks. The Greeks prided themselves on their bodies and their control over nature, and were defeated by the Jews who worship the Creator who commands nature.

This thesis is *not* a celebration of man's ability to control nature, but rather an acknowledgement of man's ability to be awed by nature and its workings. The Talmud (Shabbat 75a) calls it a commandment to understand and study the workings of creation, basing itself on the verse in Isaiah (5:12). It goes so far as to advise against speaking to one who has the ability to study and understand the marvels of creation and chooses not to pursue these interests. While, most commentaries (see R' Asevilli and Maimonides) do not count this as one of the 613 commandments, the Behag does.

Aharon, you are young now and experiencing nature for the first time. Do not get bored with it, because there is always something new to discover. But also realize what is important in life. As your *Savta* (Heb. grandmother) wrote to me and my siblings in her thesis, keep your faith in yourself and the One above, and you will succeed in whatever you do.

Table of Contents:

List of Figures:

1. Introduction:

Cancer is one of the leading causes of death in the world [1]. One major reason is that many cancers are difficult to treat, mainly because the commonly used molecular drugs are unable to reach the diseased site or cannot reach the site without being structurally modified inside the organism [2]. As a result, much effort is being devoted to the development of approaches that can directly target the cancer cells [3].

One method that has been under investigation for the past decades is the use of nanoparticles both as a delivery system for therapeutic cargos and as a direct therapeutic when their activity can be triggered externally, for example, by interaction with light. This latter approach has gained significant interest in the scientific community and is known as photothermal therapy. While some of these approaches are currently in use, there are many others still under investigation [4].

Surface plasmons, oscillations of the conduction electrons of the metal that exist at the interface between the metal and the surrounding dielectric, were predicted to by Mie in the early 20^{th} century [5]. Recently, they have become the focus of much research due to the ability of localized surface plasmons to release heat when excited by lasers of the appropriate resonant frequency. Researchers have begun to exploit the intrinsic advantages of surface plasmons to treat cancer through incorporation of metallic nanoparticles into cells. By bathing these cells with light, there is an increase in temperature inside the

cancer cells due to Joule heating of the metallic nanoparticles, which leads to apoptosis of the targeted cells [6].

2. Background:

As the fight against cancer continues, it becomes more evident that each type of cancer needs to be fought individually. Glioblastoma, the most common and aggressive type of brain tumor, is one of the deadliest forms of cancer [7]. With few exceptions, glioblastoma patients have the worst prognosis of any central nervous system malignancy. Patients with end-stage glioblastoma have a prognosis of surviving about one year [8]. One of the many, and perhaps most important, reason that glioblastoma is so deadly is its difficulty of treatment [9]. The brain, and thus the tumor within, is sequestered behind a barrier of endothelial cells connected by tight-junctions called the blood-brain-barrier (BBB). This barrier of cells keeps the brain healthy and prevents foreign organisms from invading and infecting it. The downside of this barrier is that it also keeps out the drugs that would be used to treat the cancer [10]. As a result, surgery is the main form of treatment for glioblastoma patients. Surgery, however, is not completely effective, because some cells can be left behind. This is particularly true for cancer stem cells, which are usually located at the core of the tumor mass [11]. It has been shown that these stem cells can then differentiate, giving rise again to mature cancerous cells, thus causing recurrence [12]. Therefore, surgical removal of the tumor does not solve the problem; rather it just slows it down, because the tumor will eventually regrow. Other treatments for glioblastoma include chemotherapy and radiology, which have deleterious side effects to healthy tissues and perhaps more importantly, they do not

specifically target even the diseased cells [13]. In addition, glioblastoma stem cells are resistant to the chemotherapeutics [14].

The paucity of glioblastoma treatments has forced researchers to develop methods of delivering therapy directly to the cancerous cells [15]. These delivery methods exploit the known physiological differences between healthy and cancerous cells to efficiently target the diseased tissues. One common target is the surface proteins that are overexpressed in cancerous cells while maintaining basal expression in healthy tissues [16]. By focusing the treatment only on the cancerous cells, deleterious side effects can be avoided. One method of delivery is constituted by metallic nanoparticles. Metallic nanoparticles are inert in the body, but are able to selectively deliver their payload to the targeted cells when their surfaces are functionalized with antibodies specifically recognizing membrane proteins of the diseased cell. In addition, with the proper targeting moieties, metallic nanoparticles might even be able cross the BBB [17]. Additionally, by exploiting the intrinsic and drastically different properties of metallic nanoparticles and cells, targeted delivery will also yield diagnostic information, delivering exact information on the location and size of the tumor [18].

Nanoparticles, which are particles with at least one dimension smaller than 100 nm, have unknowingly been used for millennia. Metallic nanoparticles have been employed for example to stain and color glass. Suspensions of gold nanoparticles cause the red color seen in “ruby glass” similarly to the way a suspension of silver nanoparticles is the cause of “yellow glass” [19]. Recently,

the applications of nanoparticles have expanded, from solar cells to medicinal therapeutics and everything in between [20]. The source of this development is the ability researchers now have to create, functionalize, and characterize particles better than ever before. Categories of nanoparticles include liposomes, dendritic particles, metallic particles, and polymers. Each of these categories has advantages and disadvantages. For example, liposomes are more easily absorbed by cells, while metallic nanoparticles, on their own, do not elicit adverse reactions within the body [21, 22]. As such, different types of nanoparticles are being explored as possible treatments for various types of cancers in an effort to develop more effective cancer therapeutics [23].

Initially, in the oncological sciences nanoparticles were used passively, particularly to assist with cancer imaging [19]. The inert particles would aggregate in the cancer cells and allow the cancer to be visualized. Building on this initial research, nanoparticles can now be functionalized not only to target specific tissues, but also to assist in the therapy [4].

2.1 Surface Plasmons:

The electronic properties of nanoparticles are different from those of both bulk metals and individual atoms. This transition occurs as the material decreases in size from bulk to the nanometer scale, giving rise to localized energy levels and to quantum effects, which have been the focus of the scientists' interest since their discovery.

As mentioned previously, plasmonic nanoparticles in suspension add to it intriguing colors, but it has been only within the past century and a half, with Faraday's study of colloids, and Mie's solutions to Maxwell's equation for absorption and scattering of electromagnetic radiation by spherical particles, that the field of optics has come to understand how these optical effects occur, and even more recently how to take advantage of the phenomena [24, 25, 26]. These discoveries have lead researchers in two directions: One, more basically, toward the use of metallic nanoparticles as imaging agents, and the other toward their approach as theranostic tools [18]. In the first approach, the particles are injected into the host and naturally aggregate at certain points in the body, allowing for imaging of these areas. In the second, the nanoparticles interact actively with the host, either as a drug delivery mechanism or as the basis for photothermal therapy.

The purpose of imaging, usually, is to locate the diseased tissue in the body. Cancerous tissues work well as targets, because, even passively, they take up more nanoparticles from the surrounding medium by virtue of the enhanced permeability and retention effect (EPR). This is due to the "leaky vasculature" that forms as the tumor grows. The tumor grows at a rate at which the endothelial cells cannot keep up with, creating large interstices to form in the vasculature around the tumor and enabling chemicals, which the endothelial cells would normally keep out, to diffuse into the tumor. Current research in this area includes adding targeting moieties such as proteins and antibodies to the

nanoparticles to direct them to specific areas of the body, leading to a more targeted approach to imaging.

Another property of nanoparticles that is being exploited by scientists is their ability to serve as drug delivery vectors. The structure of these nanoparticles enables the scientists to load them with drugs, thus facilitating their transport across the cell membrane into the cell, via targeted delivery made possible by the presence of surface protein targeting moieties bound to the surface of the nanoparticle [27, 28].

A third use currently under research is based on the ability of noble metallic nanoparticles, such as gold, to sustain surface plasmons. By virtue of these plasmons, when light impinges on the nanoparticles Joule heating will result as a consequence of the interaction of the plasmons with the external electromagnetic field. This effect finds uses in a variety of biomedical applications, including biosensing and cancer therapy [29, 30].

2.2 Plasmonics:

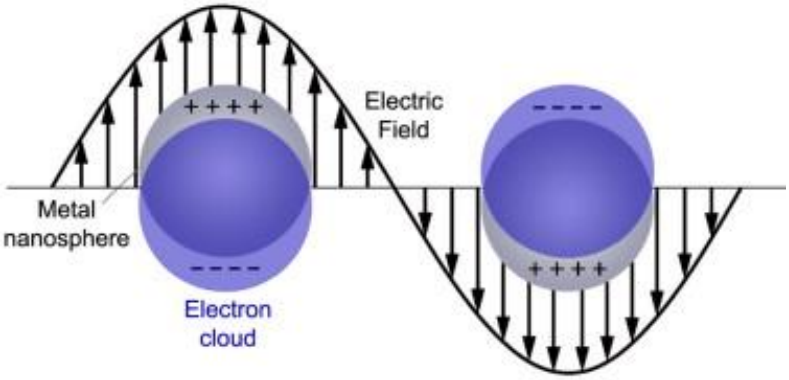

Figure 1. The interaction of nanoparticles with incoming light [31].

Plasmonic absorption works as the summation of all electric and magnetic multipole oscillations contributing to the absorption and scattering of the interacting electromagnetic field (Figure 1). When dealing with nanoparticles that are smaller than the wavelength of the absorbing light, only the dipole term is assumed to contribute to the plasmonic effect.

Giving the extinction coefficient κ, for N spherical nanoparticles within in volume V, as:

(1) $$\kappa = \frac{18\pi NV\epsilon_m^{\frac{3}{2}}}{\lambda} \frac{\epsilon_2}{[\epsilon_1+2\epsilon_m]^2+\epsilon_2^2}$$

where λ is the wavelength of the impinging radiation. ε_m is the dielectric constant of the surrounding medium, and ε_1 and ε_2 are the real and imaginary part of the dielectric function of the material.

Link *et al.* extended Mie's theory to incorporate nanorods as:

(2) $$\kappa = \frac{2\pi NV\epsilon_m^{\frac{3}{2}}}{3\lambda} \frac{1/P_j^2\epsilon_2}{\left[\epsilon_1+\frac{1-P_j}{P_j}\epsilon_m\right]^2+\epsilon_2^2}$$

where the P_j values are the depolarization factors for the three axes A, B, and C of the nanorod with A > B = C [24]:

(3) $$P_A = \frac{1-e^2}{e^2}\left(\frac{1}{2e}\ln\left(\frac{1+e}{1-e}\right) - 1\right)$$

(4) $$P_B = P_C = \frac{(1-P_A)}{2}$$

(5) $$e = \left(\sqrt{1-\left(\frac{B}{A}\right)^2} = \sqrt{1-\frac{1}{R^2}}\right)$$

Link *et al.* used these results to calculate the location of the maximum longitudinal plasmon band for a nanorod:

(6) $$\lambda max = (33.34R - 46.31)\varepsilon_m + 472.31$$

This equation lends itself to the general conclusion that the position of the longitudinal band depends on ε_m in a linear way; for a certain aspect ratio we would expect the λ_{max} to red-shift a certain amount, which is corroborated by much experimental data [32].

Another useful result from these equations is the ability to use the extinction coefficient, via the Beer-Lambert law, to determine the concentration of the sample (C) starting from experimental values such as on absorbance, A, as measured by a spectrophotometer, and path length of the absorbing medium (l):

(7) $$A = \kappa cl$$

Once the extinction coefficient (κ) is known, the concentration for a particular system can be determined. For gold nanorods, Mie's theory still has to be fine-tuned, but as with gold nanospheres, the extinction coefficient can be calculated based on size, shape, and composition, with these factors being determined by transmission electron microscopy (TEM) or scanning electron microscopy (SEM). El-Sayed has shown that by coupling TEM data and UV-Vis data allows for the development of an equation that relates the aspect ratio of rods suspended in water with an equivalent extinction coefficient [33]. These surface plasmons can be utilized in many different areas including organic solar cells and optical detection [24]. When nanorods are analyzed by a spectrophotometer a graph like the one in **Figure 2** results, with a transverse

peak at 525 nm and a longitudinal peak at a higher wavelength, depending on the aspect ratio of the rods that were analyzed.

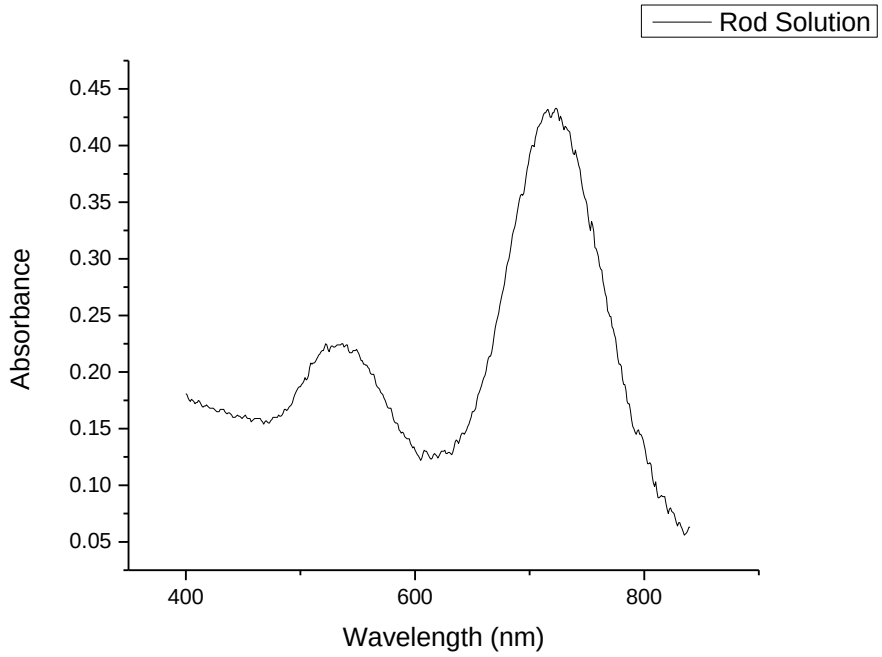

Figure 2. UV-Vis absorption spectrum of a nanorod solution.

In optical detection, plasmons can be tuned to take advantage of the near infrared (NIR) region of the electromagnetic spectrum (between 650 and 900 nm) which are known to be frequencies at which the cell and its organelles are the least opaque [34]. Recently, *in vivo* imaging of near-infrared fluorophores, red-shifted florescent proteins, and bioluminescent probes, has been demonstrated by excitation at these wavelengths [35]. Plasmons, in concert with metallic nanoparticles, have also been shown to aid in cell detection and even, exploiting photothermal therapy, to kill them [16, 4].

2.3 Cetyltrimethylammonium Bromide (CTAB):

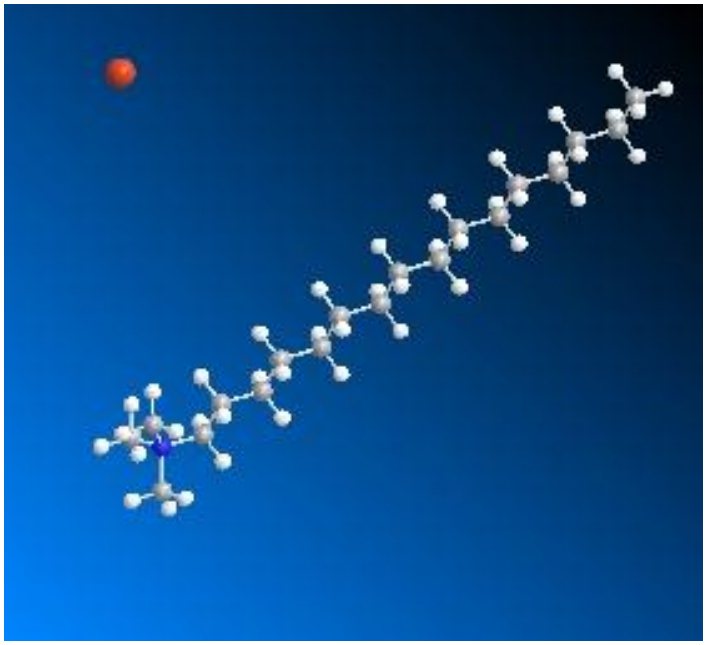

Figure 3. Ball and stick representation of the molecular structure of cetyltrimethylammonoium bromide (CTAB): The orange ball is bromide and the blue ball is nitrogen. The gray and white balls are carbon and hydrogen, respectively.

Cetyltrimethylammonium bromide (CTAB), a quaternary ammonium salt, is a surfactant. Surfactants are used to lower the surface tension of liquids, and have a structure that cannot easily be detected by conventional methods. CTAB has a 16-carbon long tail and an ammonium head group with three methyl groups attached. It was first synthesized in the mid-twentieth century and it can be used as bacterial and fungal antiseptic, as a component in buffer solutions used for the extraction of DNA, and to help condition hair [36, 37, 38].

As with any surfactant, CTAB forms micelles in solution. These micelles have an aggregation number around 80, and a critical micelle concentration of 1 mM when in water and at 25°C [39]. Usually, surfactants in aqueous solutions form spherical micelles, but some surfactants (including CTAB), further associate

into rod-like micelles with increasing surfactant concentration. In the case of ionic surfactants, rod-like micelles can only form above a certain additive salt concentration threshold. For CTAB, 0.01 M NaCl is enough to induce the formation of this rod-like micelle, with the size of the micelle increasing with the concentration of salt [40]. The shape of the micelle becomes more fluid when the micelle has a molecular weight of about 10^5 [41].

One advantage of this unusually shaped micelle is the ability to induce the growth of rod-shaped colloidal gold nanoparticles in aqueous solution [42].

2.4 Gold Nanoparticles:

Gold nanoparticles can be synthesized in solution to form spheres of different sizes depending on the type and amount of reducing agent that is added to the solution [43]. Other shapes can be obtained simply by modifying the reducing agent [44]. Typical reducing agents include sodium citrate, used for nanospheres, and ascorbic acid, used for nanorods [42]. The method used herein to develop seed-mediated gold nanorods in the presence of surfactant to help induce the shape of the gold into rods, is a multistep synthesis, based on El-Sayed's work [45]. Following this method, the reactions involved in the reduction of gold salt ($HAuCl_4$) to give metallic gold are the following:

The $HAuCl_4$ salt disproportionates when added to water:

(8) $$HAuCl_4 \rightarrow AuCl_3 + H^+ + Cl^-$$

Sodium borohydride when added to water dissociates into:

(9) $$NaBH_4 \rightarrow Na^+ + BH_3 + H^+ + e^-$$

This reduces gold to its elemental form

(10) $$Au(III) \rightarrow Au^0$$

Auric salt is reduced by the mild reducing agent ascorbic acid:

(11) $$C_6H_{12}O_6 \rightarrow C_6H_{10}O_6 + 2H^+ + 2e^-$$

Which then reduces gold:

(12) $$Au(III) \rightarrow Au(I)$$

Which is further reduced when it reaches the surface of the gold seed via electron transfer:

(13) $$Au(I) \rightarrow Au^0$$

When sodium borohydride reduces gold, the nucleation occurs. When ascorbic acid-reduced gold is added to the nucleated gold, gold growth occurs, in preferential directions. This growth is determined by the presence of the surfactant, leading to nanorods. The length of these nanorods is proportional to the amount of silver nitrate added. Murphy *et al.* assumed that silver associates with bromide causing a weakening of the CTAB micelle, thereby allowing the nucleated gold to grow in the direction of the weakened micelle [42]. The stability of the micelle arises from the bilayer of surfactant molecules that surrounds the nanorod in solution. This also prevents aggregation of the nanorods, because the micelles repel each other in solution. When the nanorods are purified through centrifugation and the CTAB concentration drops below 1 mM, the nanorods do aggregate, because CTAB cannot form micelles below its critical micelle

concentration of 1 mM. Whether the stability that the micelle lends to the nanorod is by virtue of many small micelles around the rod, or several larger micelles surrounding the rod, is still an open question [46].

2.5 Electrospray Ionization Mass Spectrometry (ESI-MS):

Electrospray ionization mass spectrometry (ESI-MS) is a relatively new analytical method discovered and championed in the early 1980's by the late John Fenn, who shared the 2002 Noble Prize in chemistry for his work on the subject [47]. ESI-MS produces large ionic macromolecules that do not fragment. The sample solution is sprayed from a small syringe into a flow of warm nitrogen gas, to assist dissolving the sample, and then into a strong electric field. The subsequently formed droplets are evaporated under a vacuum that is kept at millitorr pressure. This causes the charge to increase on the droplets. The charged droplets then enter the analyzer.

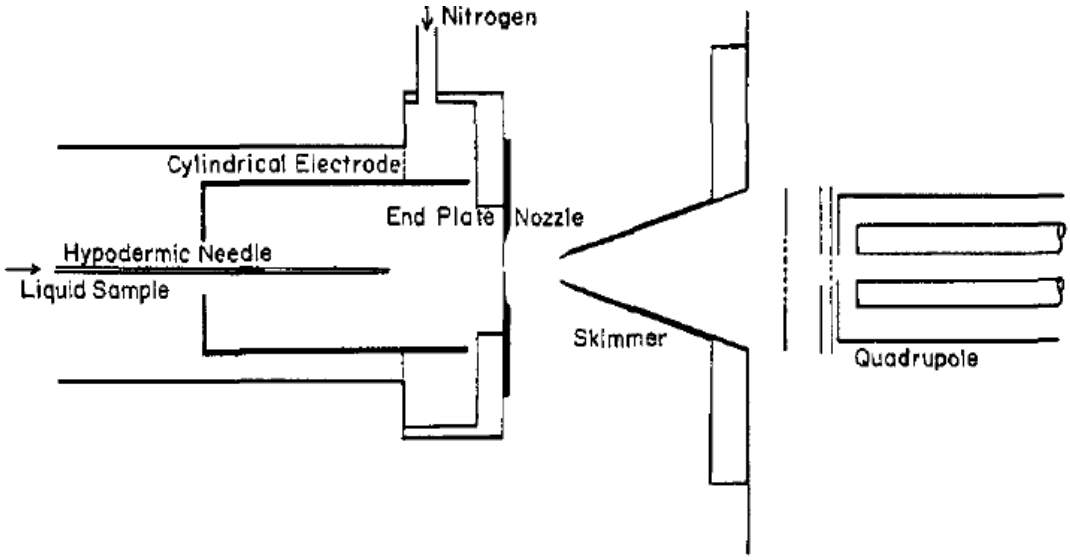

Figure 4. Electrospray ionization mass spectrometer [47].

As with all mass spectrometers, the machine gives a quantitative analysis by considering the mass-to-charge ratio of the various peaks in the spectrum. The typical ESI-MS spectrum has mass-to-charge (m/z) ratio on the abscissa and relative intensity on the ordinate. To calculate the unknown mass (M_1) from the unknown material the following equations are used.

(14) $$Peak = \frac{M}{Z}$$

(15) $$peak_1 = \frac{(M_1 + Z_1)}{Z_1}$$

(16) $$peak_2 = \left(\frac{M_1 + (Z_1 - 1)}{(Z_1 - 1)}\right)$$

where $peak_1$ and $peak_2$ are adjacent peaks and the peaks are ordered chronologically depending on their exit time, with the lower numbered peaks emerging first.

3. Aims:

Here I present a method for the detection of CTAB inside glioblastoma cells using electrospray ionization mass spectrometry (ESI-MS). CTAB will be added to the cells both alone and together with gold nanorods, to examine the mechanism by which it induces cytotoxicity. Since CTAB is required to synthesize nanorods, I will also investigate the concentration limits above which it becomes toxic.

AIM 1: Detect CTAB *in vitro*. CTAB will be dissolved in water and then incubated with cells for 24 hours, after which the cells will be washed with phosphate buffered saline (PBS) to remove any CTAB that has not been taken up by the cells. The cells will then be ruptured using a lysis buffer and centrifuged. The remains of the cells will be analyzed via ESI-MS to detect CTAB *in vitro*.

AIM 2: Determine the mechanisms of cytotoxicity of CTAB. CTAB will be incubated with cells to determine the mechanisms of its interaction with the cells most likely responsible of its toxicity.

AIM 3: Post-fabrication modification of gold nanorods. Using our understanding of CTAB chemistry we will add iodide/potassium iodine to the gold nanorods in order to modify their morphology. This will be confirmed via UV-Vis spectrophotometry and SEM. Active modification of nanorods tunes the plasmonic absorption to the wavelength that we desire, allowing for a more specific photothermal effect.

These results will work two-fold to help advance photothermal therapy to the next stage, and eventually, the bedside. Understanding how CTAB, which is integral to the development of the rods, kills cells will allow us to monitor the phenomenon, and to modify the synthetic protocols to obtain nanorods at the same level of purity and morphology but using a lower amount of surfactant. In addition, by using post-fabrication modifications of the rods we will be able to fine-tune their shape, and thus tune their plasmonic absorption, to suit our needs. Currently, once the nanorods are fabricated there is no way to alter the aspect ratio, and in turn their optical properties. The ability to fine-tune their dimensions after fabrication opens up a world of possibilities.

4. Experimental:

4.1 Materials:

Dulbecco's Modified Eagle Medium (DMEM), Fetal Bovine Serum (FBS), DMEM Non-Essential Amino Acids Solutions, and DMEM Sodium Pyruvate Solution were purchased from Invitrogen. Cells from U87 and A172 lines and lysis buffer were provided by Dr. Charles Roth of the Rutgers Department of Biomedical Engineering.

CTAB (Lot 6U3SC) and sodium borohydride were obtained from Tokyo Chemical Industry (TCI). No further purification steps were performed on CTAB, because separate experiments were performed with this batch to ascertain the critical micelle concentration (cmc), which showed that there were no impurities.

Ascorbic acid, starch (a-Amylodextrin), silver nitrate, and tetrachloroauric acid were from Acros Organics. Crystal violet was obtained from Fischer Scientific.

Potassium bromide, potassium iodide, iodine, tetrabutylammonium hydrosulfate (TBAHS) were obtained from Sigma Aldrich.

3-(4, 5-dimethylthiazol-2-yl)-2,5-diphenyltetrazolium bromide (MTT) and the formazan dilution were obtained Antibodies Online.

The ESI mass spectrometer used was a Finnigan Icq/duo Thermo Quest. The sheath gas flow rate was 30 arbitrary units, the spray voltage was 4.5 kV, the capillary temperature was 150°C, the capillary voltage was 5 V and the tube lens offset was 15 V. The flow was 50 µl/min with 50% nitrogen gas and 50%

sample. The instrument was optimized to read the peak at 284.4 (the CTA+ peak).

The 96-well plates were read with a Beckman Coulter DTX 880 multimode detector.

4.2 Synthesis of Nanorods:

Gold nanorods were synthesized using a variation of a seed-growth method reported in the literature [42]. 7.28 g of CTAB were dissolved in 200 ml 18.2 MΩ deionized water from a Millipore Milli-Q Integral 3 system. Separately, 23 mg of $NaBH_4$, 100 mg $AgNO_3$, and 900 mg of ascorbic acid were all dissolved individually in 50 ml of 18.2 MΩ deionized water. 10 ml of CTAB solution were removed from the growth solution. 4 ml of 0.025 M $HAuCl_4$ were added to the original CTAB solution. 2 ml of the $AgNO_3$ solution were then added and the solution sat at 45°C for 45 minutes.

For the seed solution: 5 ml of 0.1 M CTAB solution were mixed with 100 µl of 0.025 M $HAuCl_4$, 5 ml of 18.2 MΩ deionized water, and 600 µl of the $NaBH_4$. 4 minutes after adding the $NaBH_4$, 1.1 ml of the ascorbic acid solution and 240 µl of the seed solution were added to the growth soltution. At this point a noticeable dark pink color, which is characteristic of nanorods in solution with an aspect ratio of 4.5, was observed.

To purify the nanorods the solutions were centrifuged three times at 7500 g for 50 minutes. After each centrifugation step, the nanorods were resuspended

with water. The concentration of nanorods at this point was 6 nM, and CTAB was assumed to be 1 mM, which is the cmc of CTAB [46].

4.3 Characterization of Nanorods:

2 µl of the nanorod suspension were placed in a Thermo Scientific Nanodrop 2000 UV-Vis spectrophotometer to obtain the absorption data. SEM images were taken with the in-lens scope, or SE2 detector of a Zeiss Sigma Field Emission scanning electron microscope (FESEM).

4.4 Cell Culture:

U87 and A172 glioblastoma cells were obtained from the Rutgers Department of Biomedical Engineering. The cells were grown in a DB Falcon 25 cm^2 tissue culture treated flask with altered DMEM media and incubated in a Thermo Electron Corporation Forma Series II water jacketed incubator at 37°C and 5% CO_2. Every three to four days the media would be aspirated and replaced with 7 ml of fresh media. Cells were viewed with an Olympus CKX31 optical microscope. When the cells reached about 75% confluence of the flask, they were split.

To split the cells, the media was first aspirated from the flask. 2 ml of 1xPBS were added and aspirated to wash the cells. Next, 1 ml of trypsin-EDTA was added and aspirated. The cells were then placed in the incubator for 30 s, to allow the remaining trypsin to digest the proteins attaching the cells to the surface of the flask. 5 ml of media were then added to the flask to resuspend the

cells. 20 µl of solution were removed and mixed with 20 µl of 0.4% volume Trypan Blue and mixed to stain for dead cells. A 10 µl drop was added to a hemocytometer to count the cells. Using this number the overall amount of cells in the flask was determined.

In order to maintain the cell line, 50 µl to 200 µl of cell solution were added to 5 ml of media in a new DB Falcon 25 cm^2 tissue culture treated flask. The cycle was repeated when the cells grew to about 75% confluence of this new flask.

When experimenting on the cells, a BD Falcon 24, 48, or 96-well tissue treated polystyrene cell culture plate was used. Using the concentration obtained from the hemocytometer, 4000, 2000, 1000 cells per cm^2, were plated, respectively. Before any experiments were done, the cells were allowed to adhere to the cell culture plates for 24 hours.

4.5 Addition of CTAB to Cells (U87 and A172):

A 96-well cell culture plate was seeded with 1000 cells per cm^2 during passages 8-15 for either crystal violet staining or an MTT (3-(4, 5-dimethylthiazol-2-yl)-2,5-diphenyltetrazolium bromide) assay [48]. Crystal violet was used as live-dead staining, while MTT was used as an indicator of cell enzyme activity. In addition, a 24-well cell culture plate was seeded with 4000 cells per cm^2 for electrospray ionization.

4.6 Crystal Violet Staining:

Crystal Violet is a histological stain that is used as a live-dead cell stain.

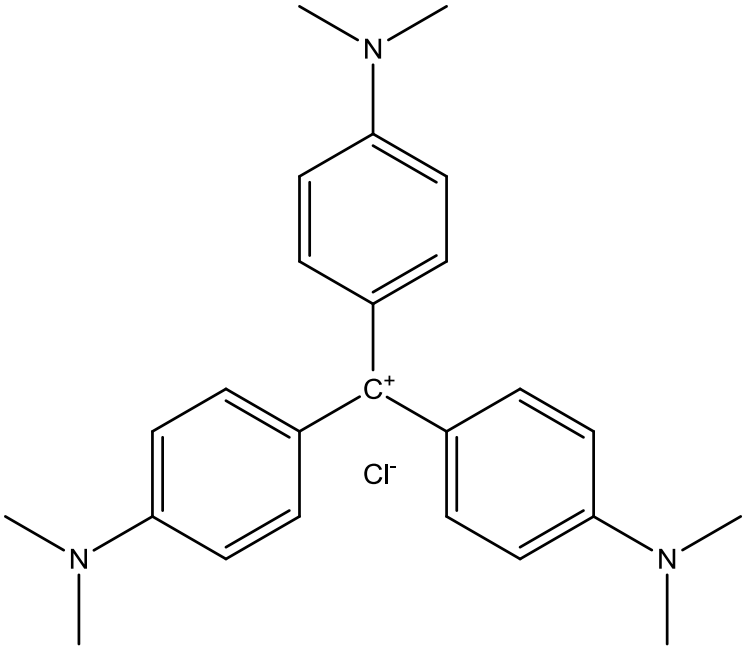

Figure 5. Molecular Structure of Tris (4-(dimethylamino)phenyl)methylium chloride.

500 mg of crystal violet (CV) were dissolved in 25 ml of methanol and 75 ml of 18.2 MΩ deionized water. This resulted in a 0.5 % CV solution. The purpose of the methanol is to fix the cells.

To stain the cells, the media was first aspirated, and the cells washed with 18.2 MΩ deionized water. The water was aspirated and 50 µl of CV were added to each well in the 96-well plate. The sample was incubated at room temperature for 10 min. The 96-well plate was then rinsed with distilled water until no more CV could be washed away. The well plate dried overnight at room temperature. After 12 hours of drying, 50 µl of 10% acetic acid solution were added to each well to read the viability results. The protocol used to read the 96-well plate prescribed to measure the absorbance at 570 nm.

4.7 MTT Assay:

After the cells have been incubated in a 96-well plate with CTAB for 24 hours, 10 µl of 3-(4,5-dimethylthiazol-2-yl)-5-(3-carboxymethoxyphenyl)-2-(4-sulfophenyl)-2H-tetrazolium (MTT) were added to each well, and the solution was further incubated for 4 hours. Then 100 µl of formazan dilution was added to each well to dissolve the insoluble product (Z,E)-5-(4,5-dimethyl-4,5-dihydrothiazol-2-yl)-1,3-diphenylformazan [49]. The wells were then read at 570 nm.

4.8 Solutions:

Table 1. Solutions, and dilutions of solutions, used throughout these experiments.

Solution name	**Composition**	**Amount of Chemical**	**Amount of Water**	**Dilutions**
A	1.6 mM TBAHS	10.865 mg	20 ml	Stock
B	1.6 mM CTAB	11.668 mg	20 ml	Diluted to 0.8 mM.
C	0.4 mM KBr	0.95 mg	20 ml	Stock
D	0.4 mM CTAB	2.92 mg	20 ml	Diluted to 0.2mM, 0.1mM, 0.05 mM
E	1.36 mM I_2 8.16 mM KI	0.036 mg 0.135mg	100ml	Diluted to 0.34 mM I_2/2.04 mM KI
F	87 mM starch	281.1 mg	20 ml	Stock

5. Results:

5.1 ESI-MS:

Due to its chemical structure, CTAB's concentration in solution cannot be measured by conventional methods. In an effort to overcome this challenge, I used ESI-MS to analyze CTAB concentration in water. I chose ESI-MS because it is able to analyze large molecules without causing fragmentation. In order to determine if there is CTAB in a sample, a calibration curve was created analyzing solutions of CTAB in water. This experiment laid the groundwork for the rest of the experiments. Determining the detection limits of the technique was a step of paramount importance to evaluate the feasibility of the experiments.

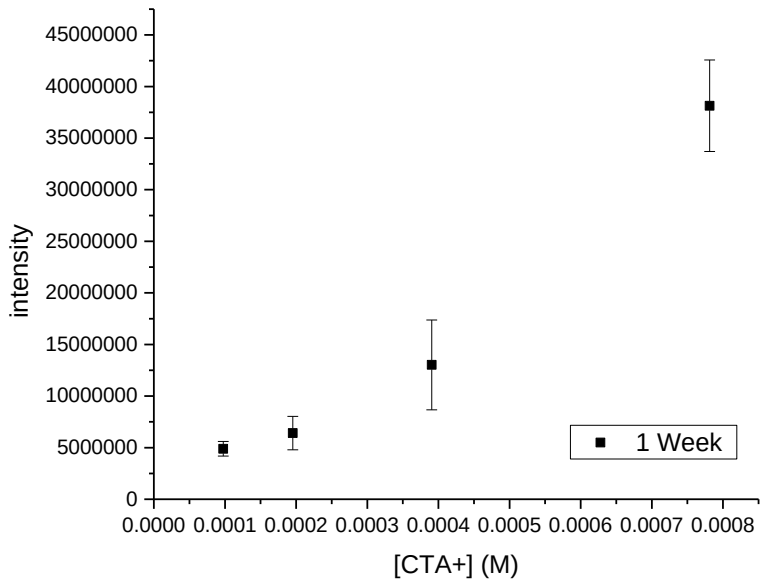

Figure 6. Results of the initial experiments run to determine the CTAB concentration in water.

CTAB was dissolved in 18.2 MΩ deionized water and diluted to 0.4 mM and 0.2 mM. The samples (n=3) were incubated at room temperature for one

month and analyzed via ESI-MS at different times during the month. One additional sample of CTAB in water at a concentration of 0.2 mM was incubated at 37°C. This was done to determine whether a change in CTA+ concentration had to be attributed to crystallization and not to time-dependent dissociation of CTAB.

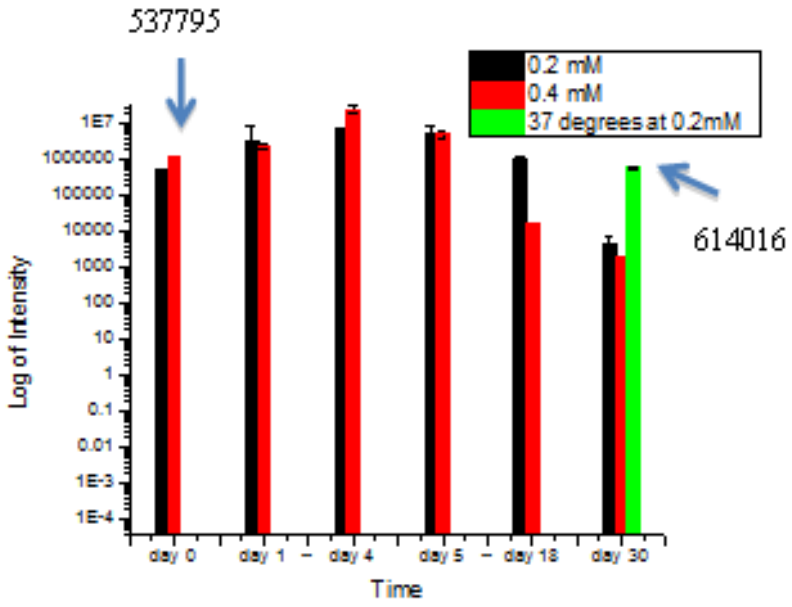

Figure 7. Log plot of intensity of CTA+ concentration in water contrasting different concentrations and different temperatures, as seen by ESI-MS.

The ESI-MS peak intensity of CTA+ at day 0 (see **Figure 6**), which was obtained from measurements collected immediately after dissolving CTAB in water and diluting it to the proper concentrations, are very similar to the intensity of the solution that was kept in an incubator for a month. The intensity for the other solutions increases until about day 5, followed by a sharp decrease, paradoxically, showing a lower concentrations of CTA+ in solutions that at the beginning contained more CTAB.

The source of this incongruity lies in the solubility of CTAB in water. CTAB's solubility in water at 25°C is much lower than CTAB dissolved in water at 37°C, and whether or not the sample crystallizes depends on its concentration [50]. Based on our experiments, only crystallization of the sample could justify the results observed. This crystallization leads initially to an increase in the local concentration of CTA+, followed by a rapid decrease happening upon CTAB precipitation. On the other hand, when the solution is kept at 37°C the crystallization doesn't occur, leading to the peaks of higher intensity observed in the ESI-MS spectra of CTA+. This is due to the dissociation equilibrium between CTAB and CTA+, that is temperature dependent.

When CTAB was sprayed inside the ESI-MS we observed an initial peak at 284.4 (**Figure 7**), which corresponds to the molecular weight of the charged ion CTA+. There are also daughter peaks that, overtime, become a larger part of the entire solution. As the ESI-MS aerosols the solution, CTAB, a neutral molecule, condenses around the charged molecules attempting to neutralize them, thereby creating larger aggregates, which give rise to the daughter peaks (**Figure 8**). This can be seen by the close up in **Figure 9**, which shows the breakdown of the peaks that surround the 648 molecular weight point. Bromine has two naturally occurring stable isotopes, with MW of 79 and 81, which give rise to the peaks at 647 and 649, respectively. The peaks at 648 and 650 are peaks 647 and 649 with an additional H^+ as occurs commonly in MS.

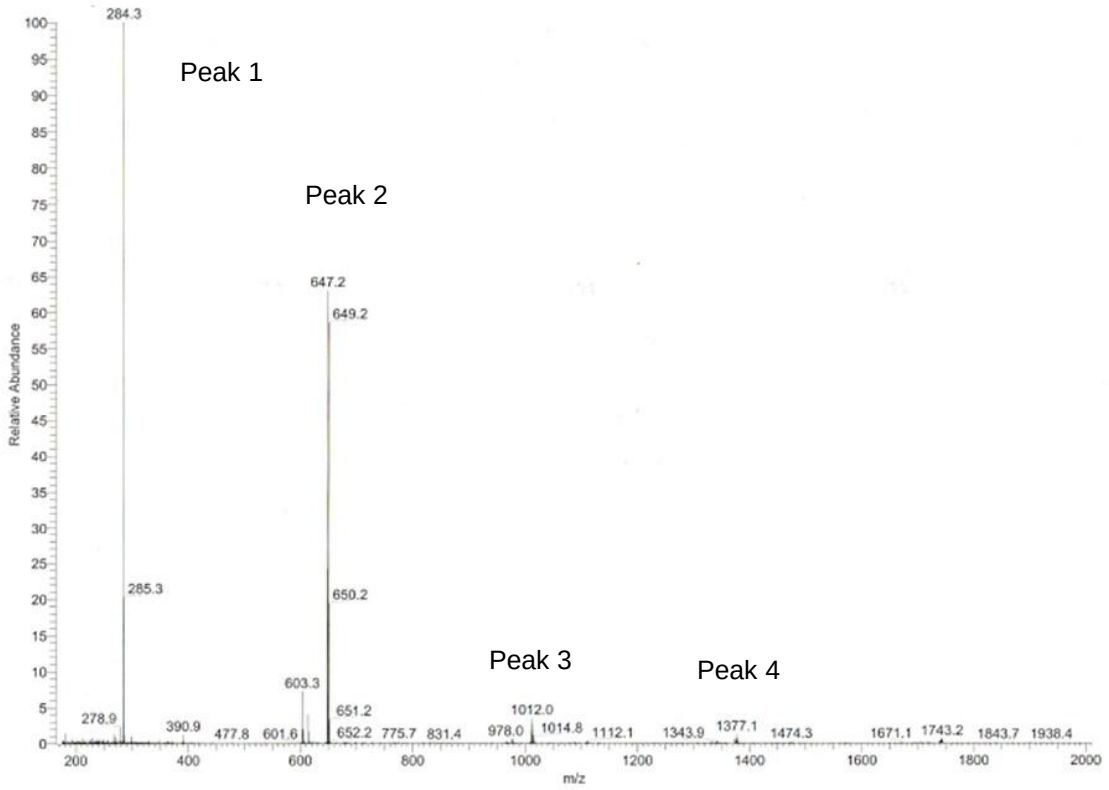

Figure 8. Typical ESI-MS spectrum of a solution of CTAB in water.

Table 2. Results of ESI-MS analysis of a solution of CTAB in water.

Peak	Molecule	Molecular Weight of Peak
1	CTA+	284.4
2	CTA+ and one CTAB molecules	647/649
3	CTA+ and two CTAB molecules	1,010/1,012/1,014
4	CTA+ and three CTAB molecules	1,373/1,375/1,377/1,379

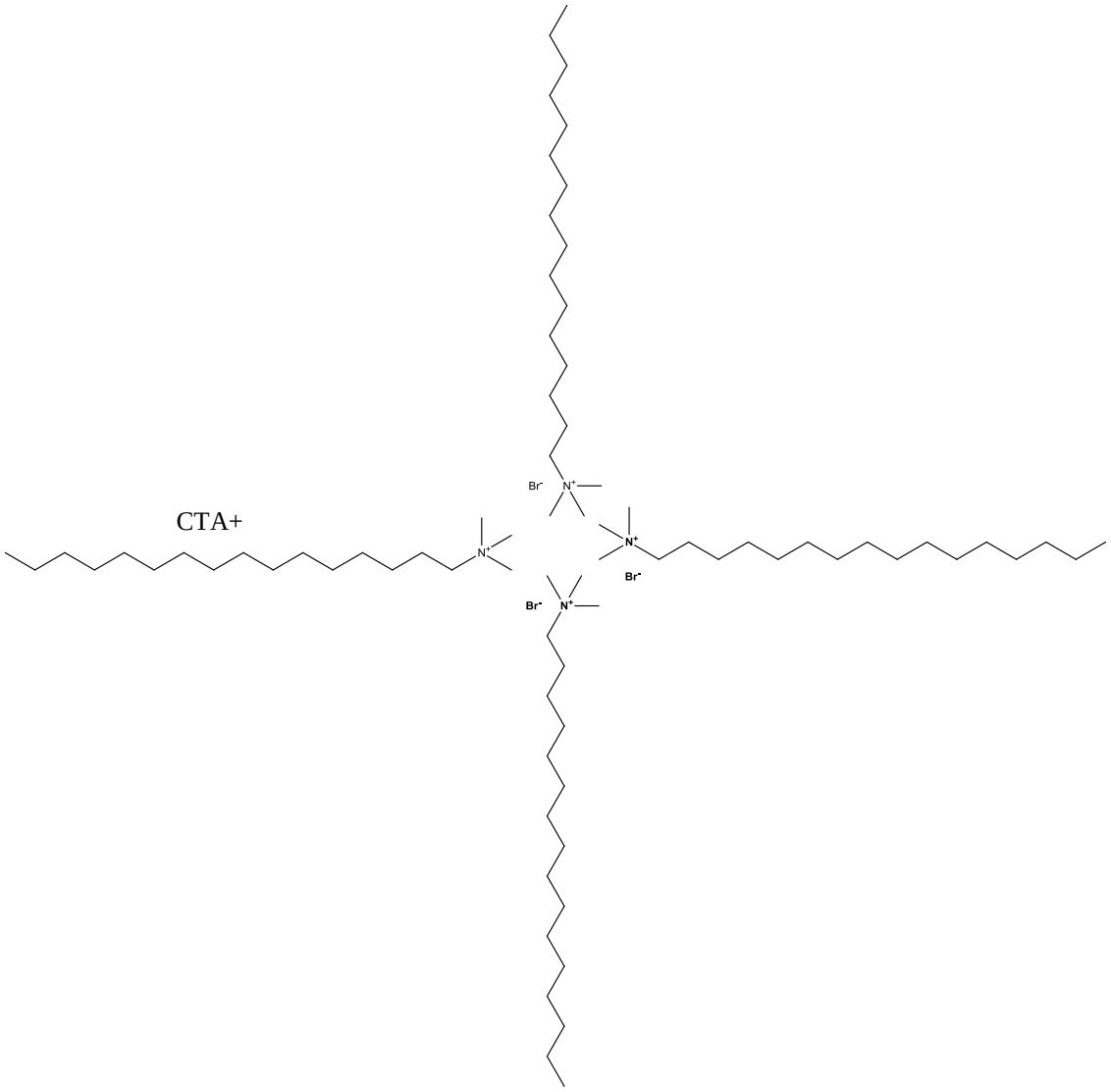

Figure 9. Assumed structure of CTAB coalescing around the charged CTA+ ion to shield or neutralize the charge.

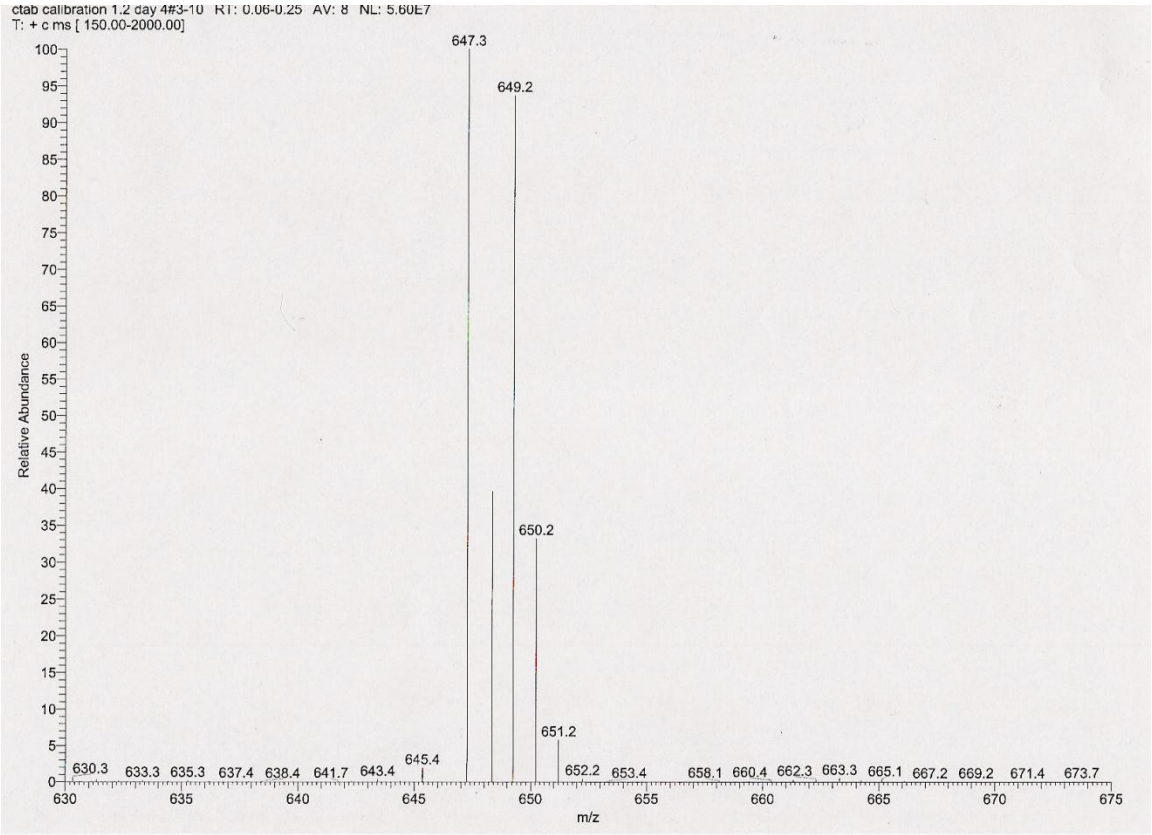

Figure 10. Close-up of a typical ESI-MS spectrum. The peak evidences the splitting due to the isotopic distribution of the two main forms of bromine, Br^{79} and Br^{81}.

5.2 Crystal Violet and MTT Assays:

Once we had a method for determining the presence of CTAB in solution, and calculated the detection limits of ESI-MS for this experiment, we were able to look at the cytotoxic effects of CTAB on cells. We used two methods to look at cytotoxicity. One was crystal violet staining, which stains live cells, and the other was MTT, which shows a cell's ability to reduce small molecules. Crystal violet is used as a live-dead cell stain. It binds DNA and allows for quantification of cell viability. The MTT assay is used to show that cells are alive by demonstrating their ability to reduce MTT to a formazan, and is the golden standard for testing cell viability. The ability of MTT to be reduced is integral to cellular survival,

because without it, the cell cannot replenish its supply of NADPH and ATP –the energy molecules of the cell. Therefore, if MTT is reduced, the cell is alive, and if MTT is not reduced the cell is dead. The resulting product is insoluble in water: It is dissolved and read at 570 nm, inside the 96-well plate where the reaction took place, to show that the reaction occurred. Both methods gave similar results.

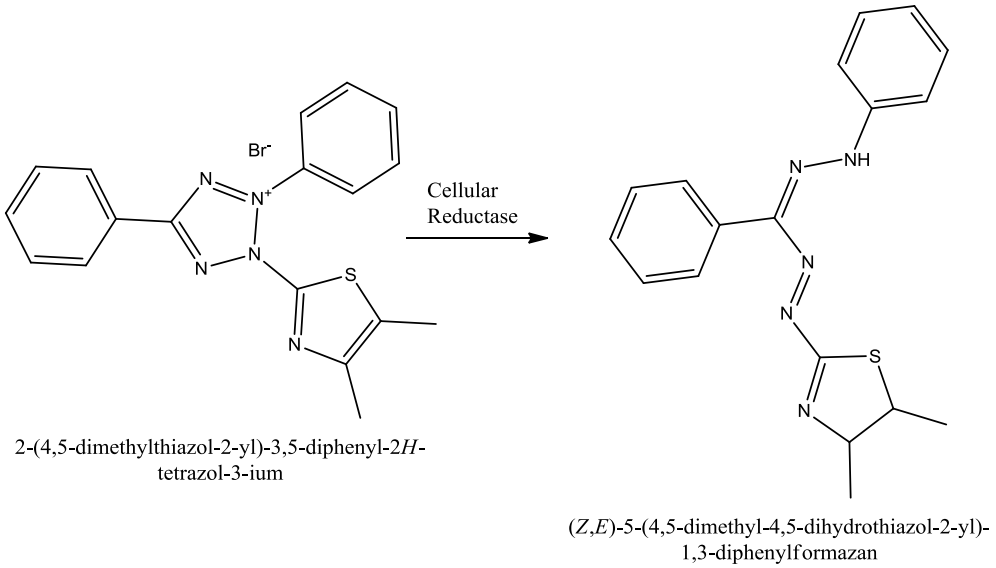

2-(4,5-dimethylthiazol-2-yl)-3,5-diphenyl-2*H*-tetrazol-3-ium

(*Z*,*E*)-5-(4,5-dimethyl-4,5-dihydrothiazol-2-yl)-1,3-diphenylformazan

Figure 11. The reaction at the basis of the MTT assay.

5.3 CTAB Incubated in Cell Lines:

In order to ascertain the source of the cytotoxicity, different concentrations of CTAB, Br-, and tetrabutylammonium hydrosulfate (TBAHS) were all incubated in both U87 and A172 cell lines. Br- is another product of CTAB dissociation, and these experiments allowed us to show that this ion does not contribute to CTAB's cytotoxicity. The experiments carried out with TBAHS had the purpose to determine its applicability as an internal standard and rule out its toxicity. In addition, it was appropriate for ESI-MS measurements of CTAB because it doesn't dissociate in water.

For clarity I will only be showing the A172 cell lines throughout this entire manuscript. Both cell lines exhibited similar behavior.

Stock solutions B and D (at 1.6 mM and 0.4 mM CTAB concentration respectively) were diluted in 18.2 MΩ water to 0.8 mM, 0.4 mM, 0.2 mM, and 0.1 mM. This dilution was done three times to carry out a statistically significant number of experiments. One set of solutions was incubated at 37°C for a month before it was used (aged CTAB at 37°C), one was made with 25°C water and used immediately (fresh CTAB at 25°C), and one set of dilutions was made with water at 37°C and used immediately (fresh CTAB at 37°C). Solution C (0.4 mM KBr) was also added to cells at the same concentration values to determine if the cytotoxicity stemmed from the free Br^- left in solution upon CTAB dissociation. Lastly, solution A (0.4 mM TBAHS) was added to the cells at concentrations of 0.4 mM and 0.2 mM. TBAHS, like CTAB, is a surfactant, and it is used to prepare buffers meant to maintain red blood cells [51]. Like CTAB, it can be analyzed by the ESI-MS, but it doesn't dissociate over time. Therefore it can be used as an internal standard, even when CTAB is added to cells, to quantify the exact amount of CTA+ in solution.

100 µl (n=3) of each solution were added to each well in a 96-well plate in addition to the 100 µl thus reducing the concentration in half: 0.4 mM, 0.2 mM, 0.1 mM, and 0.05 mM. The cells were incubated for 24 hours and then 10 µl of MTT were added to each well. The cells were incubated for an additional 4 hours, at which point 100 µl of the formazon dilution were added to each well. The plate was shaken for 10 minutes and then read at 570 nm.

Cells tended to remain alive at low concentrations of CTAB when the CTAB was made fresh and at 25°C and not incubated, as seen in **Figure 11**. When KBr was added to the cells, there was very little change in cell behavior, thus proving that CTAB's cytotoxicity is not due to Br- that is free in solution when CTAB dissociates.

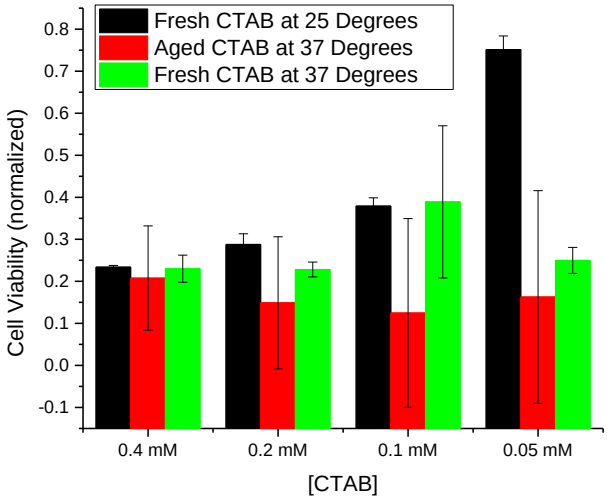

Figure 12. CTAB, aged and fresh at different temperatures and their cytotoxic effect on cells. These results are normalized to the absorbance of the control wells, containing only media and cells.

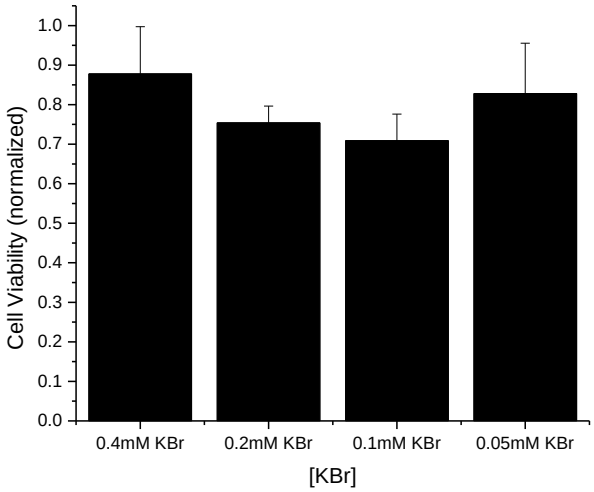

Figure 13. Result of viability tests on cells incubated with Br- at different concentrations.

6. Discussion:

Since the initial experiments analyzing the uptake of CTAB-stabilized gold nanorods by cells, the source of cytotoxicity has been a topic of much argument. The possibilities that were put forward ranged from implicating the gold as the source of the cytotoxicity to implicating the CTAB as the source, with each giving many plausible mechanisms [52]. The common consensus now is that the source of the cytotoxicity is CTAB. This was shown in an elegant, yet simple experiment. If the CTAB-nanorod solution is spun down to a pellet and two sets of cells are incubated with supernatant and the purified pellet it is possible to observe that the CTAB in the supernatant is much more fatal to cells than the gold nanorods. Despite this, gold at sizes below 5 nm is known to penetrate into the nucleus of the cell and generate reactive oxygen species induced by autocatalytic reactions at the extremely reactive surface of these small nanoparticles [53] [54] [55]. However, usually nanorods synthesized with seed-mediated methods are large than this.

Another proof that the CTAB bilayer that surrounds the nanorods is the source for the cytotoxicity is from Vigderman *et al.*'s replacement of the bilayer with a thiolated CTAB analog, (16-mercaptohexadecyl) trimethylammonium bromide (MTAB). The difference between CTAB and MTAB is that MTAB has a thiol in place of the last carbon atom at the end of the hydrocarbon chain. This thiol allows for attachment of the surfactant molecule directly to the surface of the gold nanorod, instead of being electrostatically bound to its surface in a micelle. Vigderman *et al.* showed that these MTAB-coated nanorods have very little

toxicity, because the nanorods are sequestered into vesicles inside cells, with the MTAB attached, without leaving any free surfactant in solution [56].

One of the many mechanisms that were put forth, that bears pointing out, is the charge of the surfactant and how that affects the cells. Hauck *et al.* layered different polyelectrolytes on top of the CTAB layer surrounding the gold nanorod thereby removing the possibility of CTAB causing the cytotoxicity and instead evaluating whether the charge (analyzed through zeta-potential) is the cause of the cell death. Using both positively charged and negatively charged polyelectrolytes they showed that charge is not implicated in the cell death [57].

One of the biggest drawbacks in understanding the mechanism of CTAB-stabilized nanorod cytotoxicity, is that if CTAB is implicated in causing the cell death, the amount of CTAB that is effectively inside the cell needs to be measured. Currently, the only way to do this is by serial dilutions. A solution with a certain concentration of CTAB is made and then added to cells at different concentrations to see at what concentrations the cells start to die out. For most cell lines this number hovers around the cmc, which is 1 mM. The issue is that this type of evaluation doesn't give us information on the amount of CTAB that has *effectively* penetrated the cells.

We tried to solve this problem by using ESI-MS. We chose ESI-MS because of its use in measuring large molecular weight compounds without causing them to fragment. Its drawback is that it can only measure charged particles, thus not the stabilized CTAB, but rather CTA+. The goal was to create

a calibration curve to determine the exact amount of CTA+ in a given solution, assuming that CTAB dissociates immediately upon dissolution.

Our initial results showed a peak at 284.4, which is the size of the CTA+ ion, with the intensity of the peak increasing overtime and leading us to conclude that CTAB does not immediately dissociate when dissolved in water, but that this is rather a phenomenon that occurs over time.

To test this assumption, we incubated CTAB for a month and then analyzed the sample with ESI-MS. The known initial concentration of CTAB in the incubated solution was the same as that of freshly made CTAB. Therefore, the difference in concentrations of CTA+ seen with ESI-MS is not due to an increase in CTAB's dissociation over time, but rather to its crystallization within the solution. CTAB is very soluble in water at 37°C, but not as soluble at lower temperatures. Even at low concentrations noticeable crystallization occurs. Our results must be showing that neutral CTAB is crystallizing over time which leads to a higher local concentrations of CTA+. At five days the system starts to settle out of solution, that is why we start to have a decrease in the amount of CTA+. Eventually, after a month, in the non-incubated samples of CTAB, very little CTA+ is seen, therefore showing that incubation reduces the crystallization and maintains the solubility of the CTAB in solution. The one caveat is that there is a slight increase in the amount of CTA+ in solution, but this due to its dissociation (see Equation 17), which is also temperature dependent.

(17) $$CTAB \leftrightarrow CTA^{+} + Br^{-}$$

The next step was to incubate the cells with the CTAB that had been aged inside at 37°C in an incubator and with a freshly made CTAB batch. There was a difference in the cytotoxicity profile for each of these solutions. The CTAB that was at room temperature did not kill as many cells as CTAB that had been incubated for a month. The difference was most pronounced at 0.05 mM CTAB.

Two variables could play a role in the observed cytotoxicity: 1) the temperature of the solution and 2) the age of the solution. To ascertain which the cause was, a CTAB solution was made with water at 37°C and then immediately incubated with cells for 24 hours. The results were very similar to cells that were incubated with aged CTAB that was incubated at 37°C. This showed that CTAB dissolved in warmer water is more cytotoxic than CTAB that was dissolved in water at 25°C, and that the incubation time did not influence the cytotoxic effect. Therefore, CTA+, whose concentration in solution increases at higher temperature, is the main factor that contributes to the cytotoxicity.

6.1 CTAB's Ability to Help and Hinder Cell Growth:

CTAB has been known for decades to kill cells, and a variety of mechanisms have been hypothesized over the years. 1) The CTAB micelle might be interfering with the bilayer, 2) it might be creating small holes in the phospholipid bilayer, 3) it might activate autolytic enzymes, or 4) it might create a charge inversion across the bilayer [36, 58, 59, 60]. Here we show that at sub-critical micelle concentrations (<1 mM) CTAB is still able to kill cells therefore the micelle cannot be implicated in causing the cell death. Many studies, including

one by Hauck *et al.* have shown that by surrounding the bilayer with different charged polymers the cytotoxicity can be inhibited [57].

Shimon Ulitzur did some experiments in the late 1960's with CTAB that shed a light on what we are seeing. He added CTAB at low concentrations to ML_{35} cells [61] [62]. ML_{35} cells are *E. coli* cells that have an excess of *β*-galactosidase, but do not have a suitable permease for transfer of said *β*-galactosidase. Ultizur discovered that ML_{35} cells that are incubated with sub-lethal (low) concentrations of CTAB are able to survive and the cells are rendered capable of using *β*-galactoside from the medium. But at very low concentrations the cells are unable to utilize the *β*-galactoside that is in the medium. Also, at low concentrations he was able to find 260 nm absorbing material (cell bodies) outside cells, while at very low concentration nothing at that wavelength was found in the supernatant.

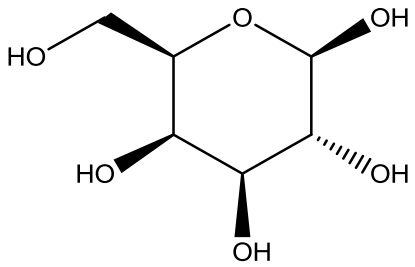

Figure 14. Molecular structure of *β*-galactoside.

These results lead Ulitzur to propose that CTAB at low concentrations is not able to make it all the way into the cell. While at slightly higher concentrations CTAB is able to create holes in the phospholipid bilayer that are few in number. These holes are not enough to kill the cells, but do allow for *β*-galactoside to penetrate into the cell (**Figure 15**).

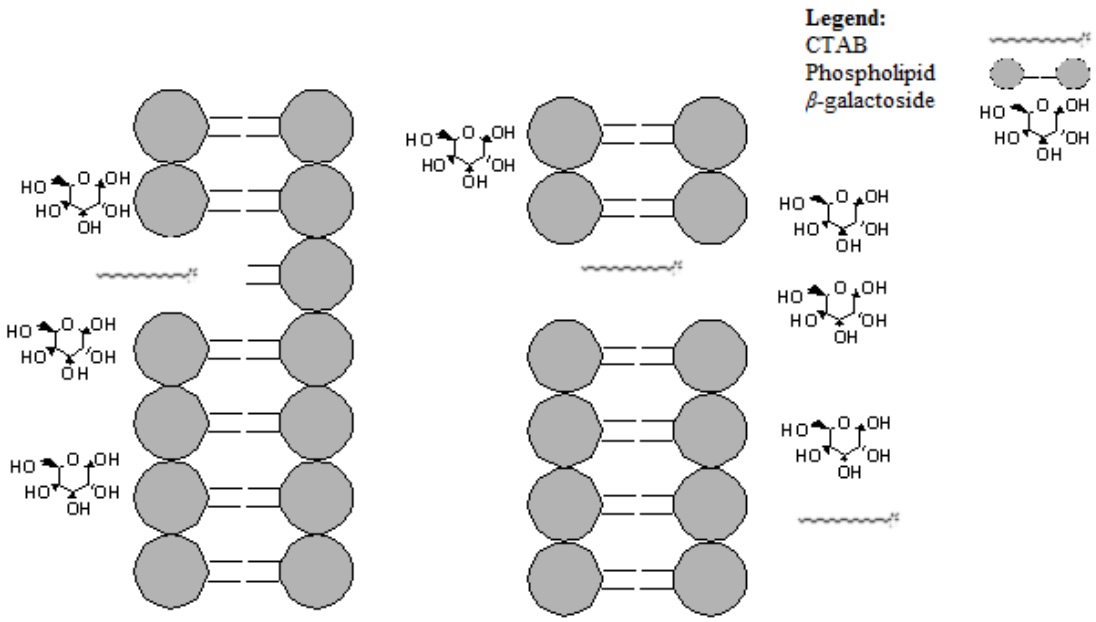

Figure 15. CTAB at very low concentrations is not able to make it through the entire phospholipid bilayer to create a hole into the cell. At higher concentrations it is able to knockout the phospholipids and create small holes into the cell. When the holes occur in the cell membrane *β*-galactoside is able to enter the cell [62].

He also found out that these results were pH-dependant. In the pH range of 6-8 there was an increase in the permeability of the membranes to *β*-galactoside. Also, this mechanism was not active in ATP-starved cells, but was reactivated upon addition of ATP to the media.

To determine if we can discover the presence of any phospholipids displaced by CTAB, we incubated cells with water. This was done because the addition of media would have led to a clogging of the ESI-MS due to the presence of serum. Despite the absence of media, the cells were kept alive long enough to run the ESI-MS experiments and observe a peak around 385.3. We tagged this peak as phosphatidylserine. At first we were only able to see a slight amount of phosphatidylserine in the supernatant, but when we incubated cells

with serum-free media and CTAB there was a large increase in the amount of phosphatidylserine within the media. We tried to find whether the amount of CTA+ in the cells was commensurate with the amount of phophatidylserine in the supernatant by lysing the cells, but the high amount of cellular bodies gave too much noise in the region of the CTA+ peak, and only at really high concentrations of CTAB were we able to find a distinct peak in the ESI-MS results.

Phosphatidylserine is a membrane phospholipid, but unlike the other phospholipids that are found throughout the membrane, phosphatidylserine is only found on the cytosolic side of the membrane. There is a dedicated membrane enzyme, called flippase, that flips phosphatidylserine back inside the cell when it encounters it on the extracellular side of the membrane [63].

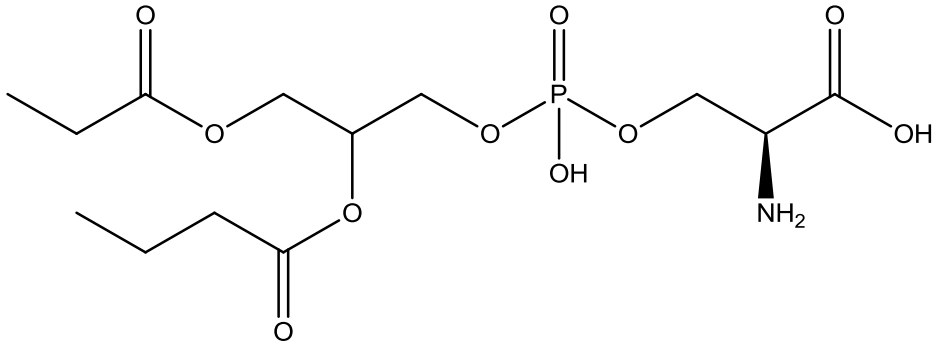

Figure 16. Molecular structure of phosphatidylserine, also known as (2S)-2-amino-3-[(2-butanoyloxy-3-propanoyloxypropoxy)-hydroxyphosphoryl]oxypropanoic acid.

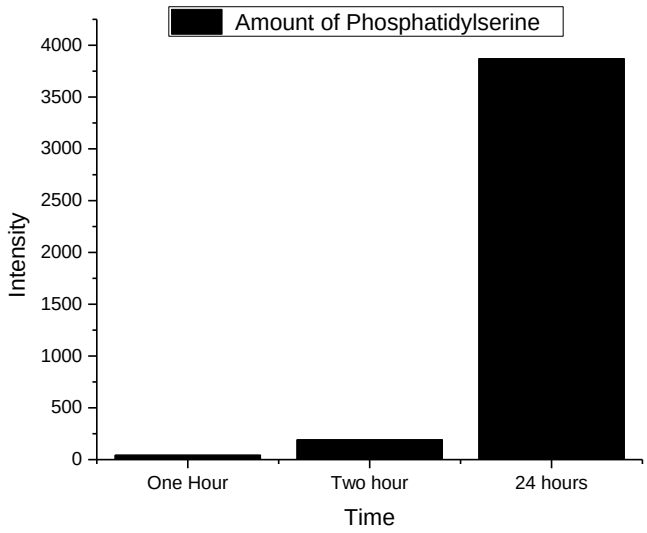

Figure 17. The increase of phosphatidylserine in the supernatant overtime.

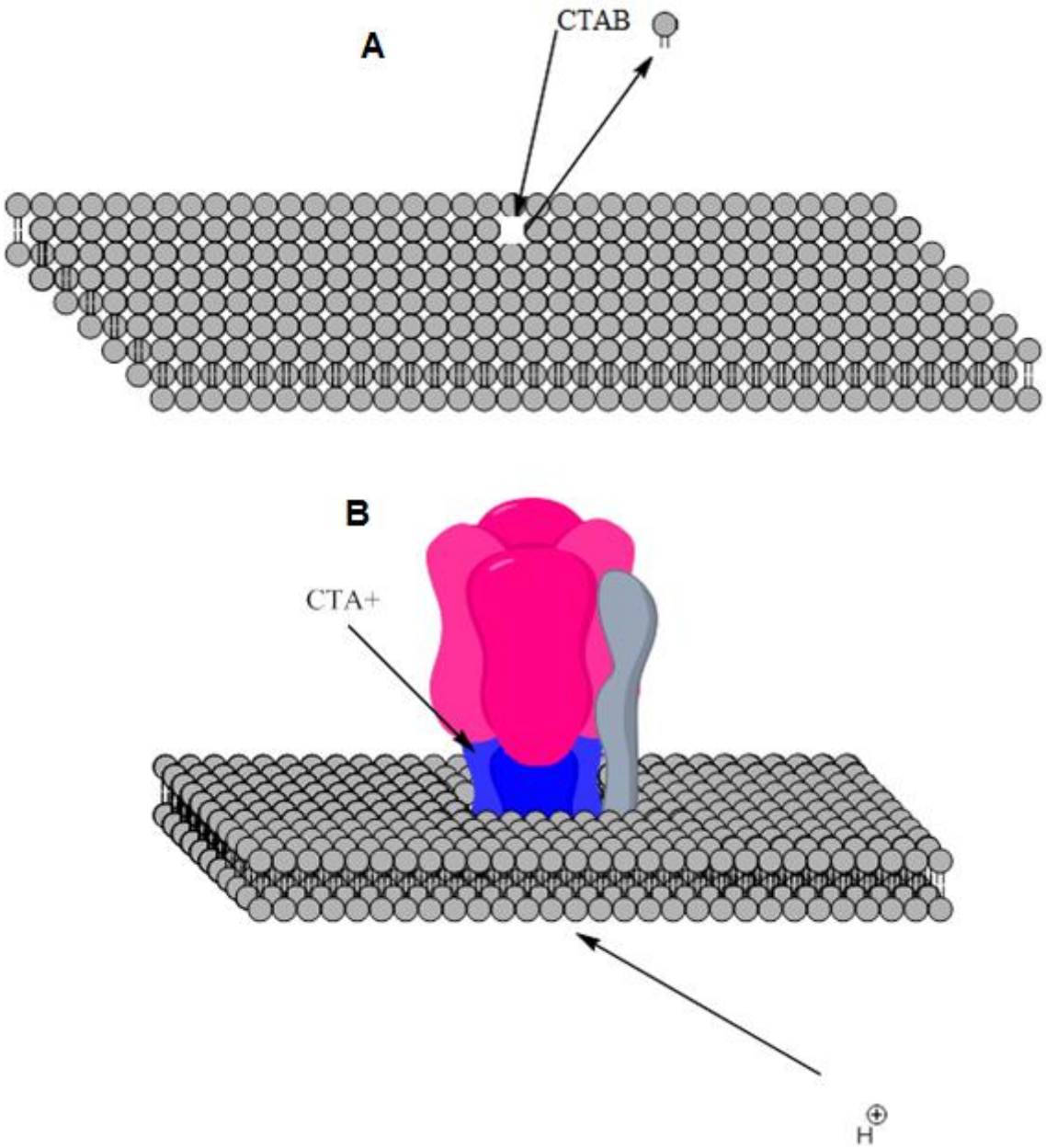

Figure 18. The two methods that we assume to be responsible for the cytotoxicity of CTAB. A) CTAB can cause phospholipids to be released from the cell membrane creating micropores. When these micropores reach a high enough concentration in the cell membrane the cells die. B) After CTA+ dissociates from Br- it is attracted by the negative charge that is used by the ATP synthase to attract H+ ions. Here, the enzyme is the integral protein, found in the mitochondria, represented in pink and blue.

Summarizing, there are two methods that we assume responsible for CTAB's cytotoxicity. In the first, CTAB displaces phospholipids along the cell

membrane, at low concentrations these holes might allow for rearrangement of the membrane and for *β*-galactoside to enter the cell, but the cell isn't killed. At higher concentrations these holes cause the cell to be too permeable and to die.

The second method of killing is based on the dissociated product of CTAB, CTA+. CTA+ is positively charged and as such it is attracted to the negative charge of the ATP synthase that is located within the mitochondrial membrane. The mechanism of action of the ATP synthase is dependent on the hydrogen ions (H+) to create ATP within the mitochondria. As the hydrogen ions flow through the channel they cause a mechanical turn within the enzyme that helps synthesize an ATP molecule. Three hydrogen ions induce one full mechanical turn of the enzyme [64]. This is why Ultizer saw a change in the cells when ATP was added to the mixture. CTA+ had stopped the synthesis of ATP, leading to cell starvation, but when external ATP was added it was able to carry-on normal cell functions because its reservoir of ATP was renewed.

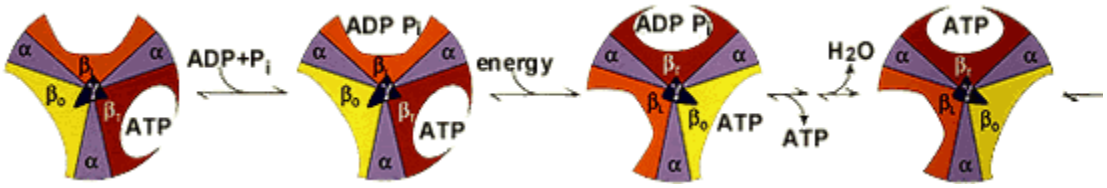

Figure 19. The ATP synthase mechanism. A full ATP is bound to β_1. Then ADP and inorganic phosphate are bound to β2. The hydrogen atom causes the enzyme to turn and thus to release ATP and bind ADP and P into ATP. Then the cycle starts over [64].

We have determined that there exist two mechanisms responsible for CTAB's cytotoxicity. The next step was to observe if they could act synergistically to give rise to cytotoxicity even at concentrations that would not normally lead to cell death in instances where the two are kept uncorrelated. At 0.2 mM the

solution, if only made of aged CTAB, is cytotoxic, but as one adds different proportions of fresh CTAB the cells do not die. This shows that there are two mechanisms that are in effect when CTAB kills the cells, one that predominates at CTAB incubated at higher temperatures and one that works at lower temperatures. They are using the same reservoir of surfactant, CTAB, but one uses it in a dissociated form while the other in the undissociated form. As one changes the proportions to higher percentages of fresh CTAB, the surfactant is all in the undissociated form, and below the concentration threshold needed to kill the cells. We also tried to add copious amounts of Br- to the CTAB solution that was incubated to take advantage of Le Chatelier's principle (increasing Br- in solution will cause the equilibrium to shift toward the undissociated form), nevertheless the cells still died. Presumably, this was due to the increase in CTAB concentration, which is also responsible for cell death.

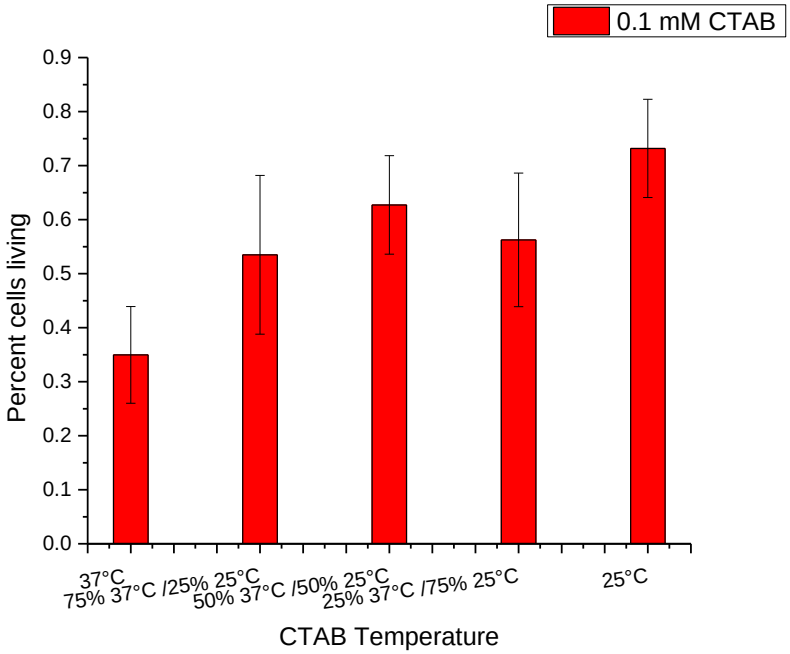

Figure 20. The results of mixing CTAB dissolved at 37°C with CTAB dissolved at 25°C and incubating with cells.

To be able to synthesize CTAB-stabilized rods that are nontoxic, concentrations of CTAB around 0.5 mM should be used. If rods are made at this concentration then previous assumptions correlating the presence of the CTAB micelle to the shape of the rods should be revisited, because this concentration is below CTAB's cmc [42]. Garg *et al.* have succeeded in preparing stable gold nanorods at these concentrations [65]. They discovered that, by controlling the concentration of externally added bromide ions, the rod shape and dimensions of the resulting Au nanoparticles can be readily controlled in the presence of only a minimum amount of CTAB. This fact evidenced that the 0.1 M amount of CTAB used in the original synthesis is not needed for the CTA+ ion, but rather to supply Br-. Their end result was that Br- concentrations between 0.05 M and 0.1 M are needed for nanorod growth.

The assumption that Br- succeeds at synthesizing rods, while no other halide is as successful, is correlated to Br- binding ability, which is however lower than that of I- [65]. Even small replacements of Br- with Cl- clearly show a detrimental effect in the growth of the nanorods [65, 66].

CTA+ is still needed by the rods to direct their shape, but it is mostly providing steric protection (i.e. inhibition of side growth) of the formed rods. CTA+ is also needed to form the bilayer around the rods once they have been fully formed. This is the reason why gold nanorods, once formed, can be purified via centrifugation while maintaining the concentration of CTAB at ca. 1 mM. That is all that is needed to form the bilayer.

7. The Role of Iodine

7.1 Background:

After having understood that very high relative concentrations of Br- are needed for nanorod formation, we wanted to determine whether we could manipulate the nanorod morphology post-synthesis. Currently, once the nanorods are formed there are no means to alter their aspect ratio. We assumed that if we could manipulate how Br- adsorbs to the gold surface, we would be able to alter the aspect ratio of the rods.

Since nanorods have first been synthesized, iodine has been determined to be deleterious to their stability for two reasons. One, iodine binds strongly to the positively charged micelles of CTAB, and two, iodide binds to the gold surface [67, 68]. Furthermore, recently many samples of CTAB have been found to contain high amounts of iodide, and in fact nanorod samples synthesized with these batches of surfactant actually contained spherical nanoparticles instead of rods [69] [70]. Scientists already exploit the ability of iodine to dissolve gold nanorods bound to the surface of the cell when carrying out inductivly coupled plasma (ICP) experiments [71]. Therefore, we wanted to determine if there is a possibility of using iodine to our advantage, and fine-tune with it the aspect ratio of the rod post-synthesis.

7.2 Results:

Gold nanoparticles are always in a dynamic equilibrium with the surfactant molecules stabilizing their surface. When added to a suspension of gold nanoparticles or nanorods, iodine disrupts this equilibrium, the surfactant desorbs from the surface, and the nanoparticle loses its shape. KI is added to the solution to help the iodide dissolve in water. In our experiments, starch was added to the solutions to quench the reaction by taking advantage of its ability to bind tightly to iodine as seen in iodine-starch indicator tests [72]. The result is the repression of the iodine-gold reaction. Solution E (I_2/KI) by itself (concentrated Iodine) and one diluted 4 times (dilute iodine) were mixed with gold in a 1:1 ratio. We then ran the iodine-gold nanorod reaction, and used starch to quench it at different points to image the reaction products at each stage.

7.3 Discussion:

When the rods were mixed with iodine, over time the rods disintegrated, with faster kinetics at higher concentrations of iodine. On the contrary, with dilute solutions even after two hours there seemed to be still some nanorods left intact. This was evident by the slight peak at about 700 nm observed in the UV-Vis spectra, indicative of a longitudinal absorption band.

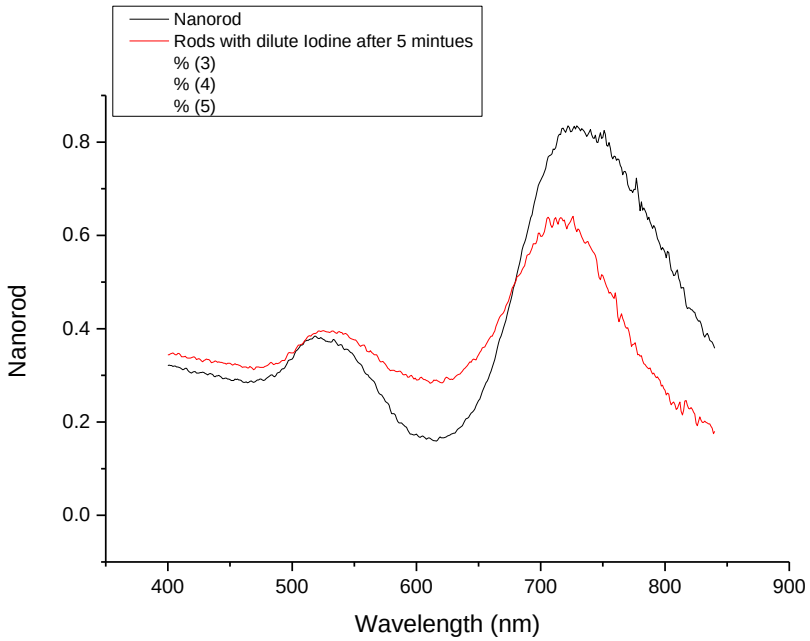

Figure 21.UV-Vis spectra of a solution of nanorods (black), and rod solutions mixed with different concentrations of iodine for different amounts of time.

We then tried to add starch into the reaction tubes to quench the reaction. **Figure 21** shows that after an initial drop there is a slight shift of the aspect ratio and an increase in the intensity of the longitudinal peak. This is indicative of a change in aspect ratio. The peak intensity of the red-shifted longitudinal peak increases as a consequence of the restructuring of the new nanords, whose concentration progressively increases. In the reaction the rods are being initially degraded by iodine, but over time iodine preferentially reacts with iodide to form I_3^- which then interacts with the CTAB in solution, thereby allowing the gold rods to reform [73].

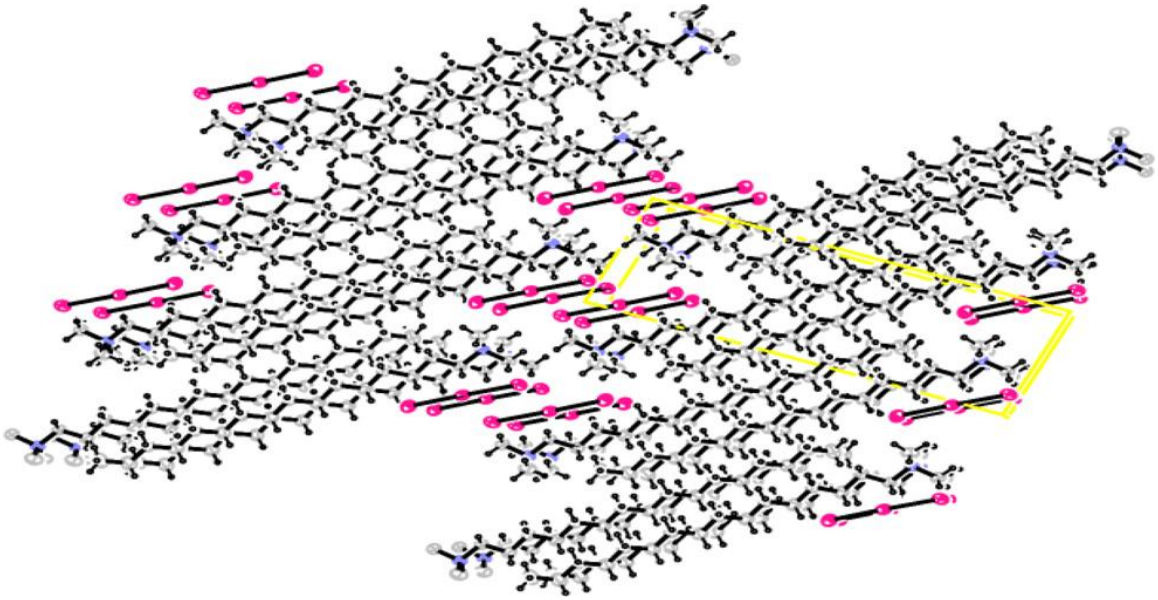

Figure 22. One possible scenario of the I_3-CTAB complex [73].

However, because the concentrations of the initial reagents have been altered during the addition of iodine and starch, the rods have now a slightly different aspect ratio. There are fewer rods than in the previous solution, but they appear to be more monodispersed, as seen by the more intense and narrower peak in the UV-Vis data. The nanorods resulting from this reconstruction have larger thickness, which is why the aspect ratio shifted and with it the optical properties of the system (**Figure 23**).

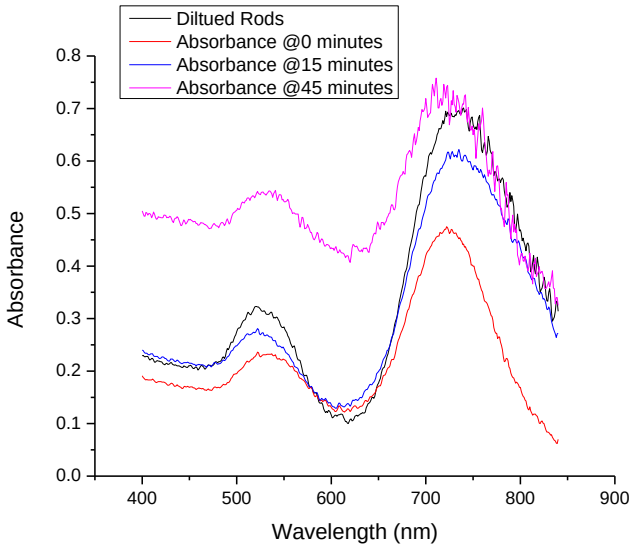

Figure 23. The iodine-gold nanorod reaction at different times.

SEM samples were also collected to quantify sample purity. There were some impurities in the sample, but of the rods that were imaged all of them followed the general trend – lower aspect ratios, but larger diameters.

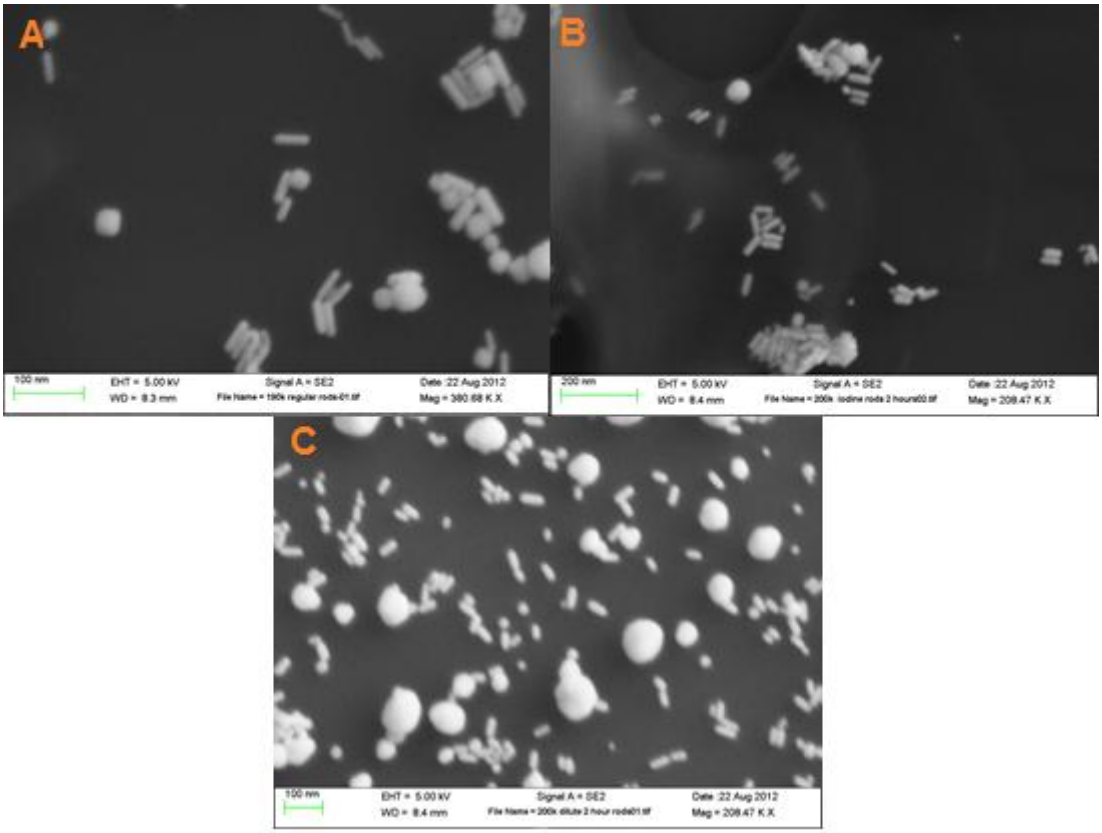

Figure 24. SEM images of gold nanorods alone, with concentrated iodine, and with dilute iodine. A is of image of normal rods. B is an image of rods mixed with concentrated iodine, and C is an image of rods mixed with dilute iodine. All were after 2 hours of incubation.

Looking forward, a series of experiments need to be carried out in order to fill in the gaps in our understanding.

Currently, the target aspect ratio of the rods is only to be within the spectral window, but that window is averaged across the entire body, with certain areas absorbing better at different wavelengths. By understanding the correlation between the amount of iodine/iodide added to the system and the change in the aspect ratio of the nanorod, we would be able to fine-tune the aspect ratio to the optimum dimensions to bring the longitudinal plasmon band in resonance with the desired wavelengths. In addition, an in-depth study of the mechanism by which iodine/iodide restructure the nanorods will be carried out, as it will significantly improve our knowledge for many different applications that exploit the interaction of light with plasmonic nanoparticles.

Not only in photothermal therapy would it be advantageous to be able to alter the nanorod aspect ratio, but also in organic solar cells. Solar cells are made to absorb light and turn it into usable energy. The most successful example of using solar energy and turning it into useable energy is photosynthesis in plants. One reason why plants are so successful is that they absorb light at several different wavelengths[1]. Although the mechanisms behind the plasmonic enhancement of organic photovoltaic devices are not yet clear, we anticipate that by having nanorods of different aspect ratios, the solar cell would be able to absorb at wavelengths that are currently not being exploited due to the intrinsic properties of the polymer active layer.

[1] This is also why plants change colors in the winter, the photo systems start to die out in the cold and the remaining ones reflect the light thereby having green leaves appear red.

Another step forward past this research would be to quantify the amount of Br- needed to be added to the system to counteract the amount (and thus the toxicity) of CTA+. Considering that CTA+ is cytotoxic at lower concentrations than CTAB, by taking advantage of Le Chatelier's principle, we can perturb the equilibrium in the system to make sure that both the concentration of CTAB and the concentration of CTA+ are below cytotoxic values, thereby allowing for the gold nanorods to be incubated directly with cells allowing for the advancement of photothermal therapy.

8. Conclusions:

CTAB is the cause of toxicity of gold nanorods. The concentration of CTA+ in a given sample can be quantified using ESI-MS. This allows for future studies to actually measure how much CTA+ is penetrating the cell, and to compensate for it. Future work also needs to be done to determine at what concnetration threshold CTA+ and CTAB actually kill cells, because the balance between dissociated and undissociated forms can be exploited to reduce CTA+ in solution. Obviously, based on these cytotoxic studies, the new method of nanorod formation, which uses much less CTAB, is highly recommended [65]. Lastly, future work also has to focus on altering the iodine/iodide system to allow for further fine-tuning of the post-fabrication nanorods. This will open up new areas of research for nanorods, because extreme fine-tuning will enable researchers to increase the specificity of the rods. This improvement will help tune lab-on-a-chip technology for biosensing and perhaps it will help increase the efficacy of photothermal therapy by finding the absolute best absorbance in the body depending on body mass of the subject and the area in the body where the tumor is found.

While the fight to cure cancer continues on its long and arduous journey, there are many sights to be seen. But even more so, are the sights that will be seen. These are the future technologies, which will be able to cure cancer better than we do now. One example of a near-future therapeutic is metallic nanoparticles and their use in photothermal therapy to kill cancer cells. It is an emerging technology, and there are still many issues that need to be dealt with,

but as time goes on more and more innovations within the field are coming out to compensate for these issues.

9. Bibliography:

1. R. Greenlee, T. Murray, S. Bolden and P. A. Wingo, *Cancer statistics, 2000*. CA A Cancer Journal for Clinicians, 2000. **50**(1): p. 7.

2. M. Ferrari, *Cancer nanotechnology: opportunities and challenges*, Nature Reviews Cancer, 2005. **5**: p. 161.

3. D. Schrama, R. Reisfeld and J. C. Becker, *Antibody targeted drugs as cancer therapeutics*, Nature Reviews Drug Discovery, 2006. **5**: p. 147.

4. El-Sayed, X. Huang and M. El-Sayed, *Surface Plasmon Resonance Scattering and Absorption of anti-EGFR Antibody Conjugated Gold Nanoparticles in Cancer Diagnostics: Applications in Oral Cancer*, Nano Letters 2005. **5**: p. 829.

5. G. Mie, *Beiträge zur Optik trüber Medien, speziell kolloidaler Metallösungen*, Annalen der Physik,1908. **330**(3): p. 377.

6. N. Matsukia, T. Ishikawa, Y. Imai and T. Yamaguchi, *Low voltage pulses can induce apoptosis*, Cancer Letters, 2008. **269**(1): p. 93.

7. Shir, M. Ogris, E. Wagner and A. Levitzki, *EGF Receptor-Targeted Synthetic Double-Stranded RNA Eliminates Glioblastoma, Breast Cancer, and Adenocarcinoma Tumors in Mice*, PLOS Medicine, 2006. **3**(1): p. 126.

8. E. Meir, C. Hadjipanayis, A. Norden, H. Shu, P. Wen and J. Olson, *Exciting New Advances in Neuro-Oncology*, CA A Cancer Journal for Clinicians, 2010. **69**(3): p. 166.

9. S. Das, J. Raizer and K. Muro, *Immunotherapeutic Treatment Strategies for Primary Brain Tumors*, Current Treatment Options in Oncology, 2008. **9**(1): p. 32.

10. J. Deeken and W. Loscher, *The Blood-Brain Barrier and Cancer: Transporters, Treatment, and Trojan Horses*, Clinical Cancer Research, 2007. **13**: p. 1663.

11. K. Wallner, J. Galicich, G. Krol, E. Arbit and M. Malkin, *Patterns of failure following treatment for glioblastoma multiforme and anaplastic astrocytoma*, International Journal of Radiation Oncology Biology Physics, 1989. **16**(6): p. 1405.

12. G. Liu, X. Yuan, Z. Zeng, P. Tunici, H. Ng, I. R. Abdulkadir, L. Lu, D. Irvin, K. L. Black and J. S. Yu, *Analysis of gene expression and*

chemoresistance of CD133+ cancer stem cells in glioblastoma, Molecular Cancer,2006. **5**(67).

13. S. Steiniger, J. Kreuter, A. Khalansky, I. Skidan, A. Bobruskin, Z. Smirnova, S. Severin, R. Uhl, M. Kock, K. Geiger and S. Gelperina, *Chemotherapy of glioblastoma in rats using doxorubicin-loaded nanoparticles*, International Journal of Cancer, 2004. **1-9**(5): p. 759.

14. Eramo, L. Ricci-Vitiani, A. Zeuner, R. Pallini, F. Lotti, G. Sette, E. Pilozzi, L. M. Larocca, C. Peschle and R. D. Maria, *Chemotherapy resistance of glioblastoma stem cells*, Cell Death and Differentiation, 2006. **13**: p. 1238.

15. K. Jain, *Use of nanoparticles for drug delivery in glioblastoma multiforme*, Expert Review, 2007. **7**(4): p. 363.

16. S. Lal, S. Clar and N. Halas, *Nanoshell-Enabled Photothermal Cancer Therapy: Impending Clinical Impact*,Accounts of chemical research, 2008. **41**: p. 1842.

17. D. Nathanson and P. Mischel, *Charting the course across the blood-brain barrier,* Journal of Clinical Investigation, 2011. **121**: p. 31.

18. X. Huang, I. H. El-Sayed, W. Qian and M. A. El-Sayed, *Cancer Cell Imaging and Photothermal Therapy in the Near-Infrared Region by Using Gold Nanorods*, Journal of the American Chemical Society, 2006. **128**: p. 2115.

19. C. Murphy, A. Gole, J. Stone, P. Sisc, A. Alkilany, E. Goldsmith and S. Baxter, *Gold Nanoparticles in Biology: Beyond Toxicity to Cellular Imaging*, Accounts of Chemical Research, 2008. **41**(12): p. 1721.

20. Mahmouda, J. Zhang, D. Ma, R. Izquierdo and V.-V. Truong, "*Optically-enhanced performance of polymer solarcells with low concentration of goldnanorods in the anodic buffer layer*, Organic Electronics*,* 2012. **13**(12): p. 3102.

21. Y. E. Rahman and B. J. Wright, *Liposomes containing chelating agents. Cellular penetration and a possible mechanism of metal removal*, Journal of Cell Biology,1975. **65**(1): p. 112.

22. D. Pissuwana, S. M. Valenzuela and M. B. Cortie, *Therapeutic possibilities of plasmonically heated gold nanoparticles*, Trends in Biotechnology, 2006. **24**(2): p. 62.

23. K. Cho, X. Wang, S. Nie, Z. Chen and D. Shin, *Therapeutic Nanoparticles for Drug Delivery in Cancer*, Clinical Cancer Research, 2008. **14**(5): p. 1310.

24. S. Link and M. El-Sayed, *Spectral Properties and Relaxation Dynamics of Surface Plasmon Electronic Oscillations in Gold and Silver Nanodots and Nanorods*, Journal of Physical Chemistry B, 1999. **103**: p. 8410.

25. M. Faraday, *The Bakerian lecture: experimental*, Philosophical Transactions of the Royal Society of London, 1857. **147**: p. 145.

26. G. Mie, *Beiträge zur Optik trüber Medien, speziell kolloidaler Metallösungen (Contribution to the Optics of Turbid Media Particularly of Colloidal Metal Solutions),* Annals of Physics, 1908. **330**: p. 377.

27. D. Schachter and J. Kohn, *A synthetic polymer matrix for the delayed or pulsatile release of water-soluble peptides*, Journal of Controlled Release, 2002. **78**(1-3): p. 143.

28. L. Juillerat-Jeanneret, *The targeted delivery of cancer drugs across the blood–brain barrier: chemical modifications of drugs or drug-nanoparticles?,* Drug Discovery Today, 2008. **13**(23/24): p. 1099.

29. M. Pumera, J. Wang, E. Grushka and R. Polsky, *Gold Nanoparticle-Enhanced Microchip Capillary Electrophoresis*, Analytical Chemistry, 2001. **73**: p. 5625.

30. C.-K. Yang, *Two dimensional simulation on immunoassay for a biosensor with applying electrothermal effect*, Applied Physics Letters, 2007. **91**(11): p. 113904.

31. C. Cobley and Y. Xia, *Engineering the properties of metal nanostructures via galvanic replacement reactions*, Materials Science and Engineering: R: Reports, 2010. **70**: p. 44.

32. L. Gou and C. Murphy, *Fine-Tuning the Shape of Gold Nanorods*, Chemistry of Materials, 2005. **17**(14): p. 3668.

33. X. Huang, S. Neretina and M. El-Sayed, *Gold Nanorods: From Synthesis and Properties to Biological and Biomedical Applications*, Adcanced Materials, 2009. **21**(48): p. 4880.

34. P. Hildebrandt, *A Spectral Window to the Cell*, Angewandte Chemie International Edition,2010. **27**: p. 4540.

35. R. Weissleder, *A clearer vision for in vivo imaging*, Nature Biotechnology, 2001. **19**: p. 316.

36. M. Thelestam and R. Mollby, *Classification of MIcrobial, Plant, and Animal Cytolysins based on their Membrane-Damaging Effects on Human Fibroblasts*, Biochimica et biophysica acta, 1979. **557**: p. 156.

37. H. Nazir, P. Lv, L. Wang, G. Lian, S. Zhu and G. Ma, *Uniform-sized silicone oil microemulsions: Preparation, investigation of stability and deposition on hair surface,* Journal of Colloid and Interface Science, 2011. **364**(1): p. 56.

38. E. M. Möller, G. Bahnweg, H. Sandermann and H. H. Geiger, *A simple and efficient protocol for isolation of high molecular weight DNA from filamentous fungi, fruit bodies, and infected plant tissues*, Nucleic Acids Research, 1992. **20**(22): p. 6115.

39. F. Quirion and L. Magid, *Growth and Counterion Binding of Cetyltrimethylammonium Bromide Aggregates at 25 C: A Neutron and Light Scattering Study*, Journal of Physical Chemistry, 1986. **90**: p. 5435.

40. T. Imae, R. Kamiya and S. Ikeda, *Formation of Sphereical and Rod-like Micelles of Cetyltrimethylammmonium Bromide in Aqueous NaBr Solutions*, Journal of Colloid and Interface Science, 1985. **108**(1): p. 215.

41. T. Imae and S. Ikeda, *Characteristics of rodlike micelles of cetyltrimethyelammonium chloride in aqueous NaCl solutions: their flexibly and the scaling laws in dilute and semi dilute regimes,* Colloid and Polymer Science, 1987. **265**: p. 1090.

42. N. Jana, L. Gearheart and C. Murphy, *Wet Chemical synthesis of High Aspect Ratio Cylindrical Gold Nanorods*, Journal of Physical Chemistry B, 2001. **105**: p. 4065.

43. G. Frenz, *Controlled Nucleation for the Regulation of the Particle Size in Monodisperse Gold Suspensions,* Nature Physical Science, 1973. **241**: p. 20.

44. M. Grzelczak, J. Pérez-Juste, P. Mulvaney and L. M. Liz-Marzán, *Shape Control in Nanoparticle Synthesis*, Chemical Society Reviews, 2008. **9**: p. 1783.

45. B. Nikoobakht and M. El-Sayed, *Preparation and Growth Mechanism of Gold Nanorods (NRs) Using Seed-Mediated Growth Method,* Chemical Materials, 2003. **15**: p. 1957.

46. C.-C. Huang, C.-H. Huang, I.-T. Kuo, L.-K. Chau and T.-S. Yang, *Synthesis of silica-coated gold nanorod as Ramantags by modulating cetyltrimethylammonium bromide concentration*, Colloids and Surfaces A: Physiochemical and Engineering Aspects, 2012. **409**(5): p. 61.

47. M. Yamashita and J. Fenn, *Electrospray Ion Source. Another Variation on the Free-Jet Theme,* Journal of Physical Chemistry, 1984. **88**(20): p. 2240.

48. T. Mosmann, *Rapid colorimetric assay for cellular growth and survival: Application to proliferation and cytotoxicity assays*, Journal of Immunological Methods, 1983. **65**(1-2): p. 55.

49. Y. Liu, D. A. Peterso, H. Kimura and D. Schubert, *Mechanism of Cellular 3- (4,5-Dimethylthiazol-2-yl) -2,5-Diphenyltetrazolium Bromide (MTT) Reduction*, Journal of Neurochemistry, 1997. **69**(2): p. 581.

50. Y. Liguo and Z. Yanhua, *Preparation of Nano-Silver Flake by Chemical Reduction Method,* Rare Metal Materials and Engineering, 2010. **39**(3): p. 401.

51. L. MacNeil, L. Hill, D. MacDonald, L. Keefe, J. Cormier, D. Burke and T. Smith-Palmer, *Analysis of creatine, creatinine, creatine-d3 and creatinine-d3 in urine, plasma, and red blood cells by HPLC and GC–MS to follow the fate of ingested creatine-d3*, Journal of Chromatography B, 2005. **827**(2): p. 210.

52. Alkilany and C. Murphy, *Toxicity and cellular uptake of gold nanoparticles: what we have learned so far*?, Journal of Nanoparticle Research, 2010. **12**: p. 2313.

53. N. Pante and U. Aebi, *Sequential Binding of Import Ligands to Distinct Nucleopore Regions During Their Nuclear Import*, Science, 1996. **273**: p. 1729.

54. Alkilany, P. Nagaria, C. Hexel, T. Shaw, C. Murphy and M. Wyatt, *Cellular Uptake and Cytotoxicity of Gold Nanorods: Molecular Origin of Cytotoxicity and Surface Effects*, Small, 2009. **5**(6): p. 701.

55. J. Coulter, S. Jain, J. O'Sullivan, G. Schettino, F. Currell, D. Hirst, K. Prise, K. Butterworth, L. Taggart, G. Dickson, S. McMahon, W. Hyland, M. Muir, C. Trainor and A. Hounsell, *Cell type-dependant uptake, localization and cytotoxicity of 1.9nm gold nanoparticles,* International Journal of Nanomedicine, 2012. **7**: p. 2673.

56. L. Vigderman, P. Manna and E. Zubarev, *Quantitative Replacement of Cetyl Trimethylammonium Bromide by Cationic Thiol Ligands on the*

Surface of Gold Nanorods and Their Extremely Large Uptake by Cancer Cells, Angewandte Chemie, 2012. **124**: p. 6.

57. T. Hauck, A. Ghazani and W. Chan, *Assessing the Effect of Surface Chemistry on Gold Nanorod Uptake, Toxicity, and Gene Expression in Mammalian Cells*, Small, 2008. **1**: p. 153.

58. D. Vieira and A. Carmona-Ribeiro, *Cationic Lipids and Surfactants as Antifungal Agents: Mode of action*, Journal of Antimicrobial Chemotherapy*,*2006. **58**: p. 760.

59. E. Ito, K. Yip, S. Kelley, F.-F. Liu, D. Katz, S. Fonseca, D. Hedley, S. Chow, G. Xu, T. Woos, C. Bastiautto and A. Schimmer, *Potential Use of Cetrimonium Bromide as an Apoptosis- Promoting Anticancer Agent for Head and Neck Cancer*, Molecular Pharmacology, 2009. **76**(5): p. 969.

60. Dawson, I. Lominski and H. Stern, *An Electron-Microscope Study of the Action of Cetyl-Trimethyl-Ammonium Bromide on Staphlococcus Aureus,* The Journal of Pathology and Bacteriology, 1953. **66**(2): p. 513.

61. S. Ulitzur, *Cation repair of Toluene-Treated Escherichia Coli ML35 Cells and the Transport*, Biochimica et biophysica acta, 1970. **211**: p. 542.

62. S. Ulitzur, *The transport of B-Galactosides across the Membrane of Permeaseless Escherichia Coli ML35 cells after Treatment with Cetyltrimethylammonium Bromide*, Biochimica et biophysica acta, 1970. **211**: p. 533.

63. M. Yabas, C. Teh, S. Frankenreiter, D. Lal, C. Roots, B. Whittle, D. Andrews, Y. Zhang, N. Teoh, J. Sprent, L. Tze, E. Kucharska, J. Kofler, G. Farell, S. Bröer, C. Goodnow and A. Enders, *ATP11c is critical for phosphatidylserine internalization and B lymphocyte differentiation,* Nature Immunology*,* 2011. **12**(5): p. 441.

64. P. Boyer, *The binding change mechanism for ATP synthase -Some Probabilities and Possibilities*, Biochimica et Biophysica Acta (BBA) - Bioenergetics, 1993. **1140**(3): p. 215.

65. N. Garg, C. Scholl, A. Mohanty and R. Jin, *The Role of Bromide Ions in Seeding Growth of Au Nanorods*, Langmuir, 2010. **26**(12): p. 10271.

66. S. Praharaj, S. Panigrahi, S. Basu, S. Pande, S. Jana, S. K. Ghosh and T. Pal, *Effect of bromide and chloride ions for the dissolution of colloidal gold,* Journal of Photochemistry and Photobiology A: Chemistry, 2007. **187**(2-3): p. 196.

67. Cuccovia and H. Chaimovich, *Determination of Micromolar Concentrations of Iodine with Aqueous Micellar Hexadecyltrimethylammonium Bromide*, Analytical Chemistry*,* 1982. **54**(4): p. 789.

68. J. Millstone, W. Wei, M. Jones, H. Yoo and C. Mirkin, *Iodide Ions Control Seed-Mediated Growth of Anisotropic Gold Nanoparticles*, Nano Letters, 2008. **8**(8): p. 2526.

69. D. Smith, N. Miller and B. Korgel, *Iodide in CTAB Prevents Gold Nanorod Formation,* Langmuir, 2009. **25**(16): p. 9518.

70. R. Rayavarapu, C. Ungureanu, P. Krystek, T. Leeuwen and S. Manohar, *Iodide Impurities in Hexadecyltrimethylammonium Bromide (CTAB) Products: Lot−Lot Variations and Influence on Gold Nanorod Synthesis*, Langmuir, 2010. **26**(7): p. 5050.

71. E. Cho, J. Xie, P. Wurm and Y. Xia, *Understanding the Role of Surfae Charges in Cellular Adsorption versus Internalization by Selectively Removing Gold Nanopartilces on the Cell Surface with a I2/KI Etchant*, Nano Letters, 2009. **9**(3): p. 1080.

72. G. W. Pucher, C. S. Leavenworth and H. B. Vickery, *Determination of Starch in Plant Tissues*, Analytical Chemistry, 1948. **20**(9): p. 850.

73. G. Das, B. Das, N. Sarma and O. Medhi, *Synthesis, structure, and properties of cetyltrimethylammonium polyiodides*, Polyhedron, 2012. **37**(14): p. 14.

74. T. Hauck, A. Ghazani and W. Chan, *Assessing the Effect of Surface Chemistry on Gold Nanorod Uptake, Toxicity, and Gene Expression in Mammalian Cells*, Small, 2008. **4**(1): p. 153.

75. S. Eustis and M. El-Sayad, *Why gold nanoparticles are more precious than pretty gold: Noble metal surface plasmon resonance and its enhancement of the radiative and nonradiative properties of nanocrystals of different shapes,* Chemical Society Reviews, 2006. **35**: p. 209.

76. N. Jana, L. Gearheart and C. Murphy., *Wet Chemical syntheis of High Aspect Ratio Cylindrical Gold Nanorods,* Journal of Physical Chemistry B, 2001. 105(19): p. 4065.